

Origin of model fractional Chern insulators in all topological ideal flatbands: Explicit color-entangled wave function and exact density algebra

Jie Wang^{1,2,3,*}, Semyon Klevtsov⁴, and Zhao Liu^{5,†}

¹Center of Mathematical Sciences and Applications, Harvard University, Cambridge, Massachusetts 02138, USA

²Department of Physics, Harvard University, Cambridge, Massachusetts 02138, USA

³Center for Computational Quantum Physics, Flatiron Institute, 162 5th Avenue, New York, New York 10010, USA

⁴IRMA, Université de Strasbourg, UMR 7501, 7 rue René Descartes, 67084 Strasbourg, France

⁵Zhejiang Institute of Modern Physics, Zhejiang University, Hangzhou 310027, China



(Received 22 November 2022; revised 14 March 2023; accepted 21 March 2023; published 16 June 2023)

It is commonly believed that nonuniform Berry curvature destroys the Girvin-MacDonald-Platzman algebra and as a consequence destabilizes fractional Chern insulators. In this work, we disprove this common lore by presenting a theory for all topological ideal flatbands with nonzero Chern number \mathcal{C} . The smooth single-particle Bloch wave function is proven to admit an exact color-entangled form as a superposition of \mathcal{C} lowest Landau level type wave functions distinguished by boundary conditions. Including repulsive interactions, Abelian and non-Abelian model fractional Chern insulators of Halperin type are stabilized as exact zero-energy ground states no matter how nonuniform the Berry curvature is, as long as the quantum geometry is ideal and the repulsion is short-ranged. The key reason is the existence of an emergent Hilbert space in which Berry curvature can be exactly flattened by adjusting the wave function's normalization. In such space, the flatband-projected density operator obeys a closed Girvin-MacDonald-Platzman type algebra, making exact mapping to \mathcal{C} -layered Landau levels possible. In the end, we discuss applications of the theory to moiré flatband systems, with a particular focus on the fractionalized phase and the spontaneous symmetry-breaking phase recently observed in graphene-based twisted materials.

DOI: [10.1103/PhysRevResearch.5.023167](https://doi.org/10.1103/PhysRevResearch.5.023167)

I. INTRODUCTION

Flatbands are ideal platforms for realizing exotic quantum phases of matter. Of particular interest are topological flatbands where fractionalized topological phases are possible [1–7]. During recent years, there has been much progress in creating and engineering flatband systems such as by stacking and twisting [8–11]. Understanding the stability of fractionalized phases with respect to tuning parameters such as energy dispersion, wave-function geometry, and interaction range is crucial for material engineering, experimental realization, and theoretical characterization of these exotic phases. Along this path, exact statements are particularly important. In this work, we present an exact condition for the stability of fractional Chern insulators (FCIs), i.e., the lattice version of fractional quantum Hall (FQH) states [3–7]. Our results also provide a framework to systematically explore the interplay between the wave function's geometry and interactions, and they are

useful in guiding material engineering toward realizing exotic quantum phases of matter.

Landau levels (LLs) are the simplest topological Chern flatbands, with unit Chern number $\mathcal{C} = 1$ and exactly zero bandwidth. They are well known for their extreme uniformness, which is crucial for the stability of FQH states: LLs are covariant under any smooth area-preserving deformations [12,13], which is encoded in the LL projected density algebra initially noticed by Girvin, MacDonald, and Platzman (GMP) for lowest Landau level (LLL) states [14,15]:

$$[\hat{\rho}_{q_1}, \hat{\rho}_{q_2}] = (e^{q_1^* q_2 l_B^2} - e^{q_1 q_2^* l_B^2}) \hat{\rho}_{q_1 + q_2}, \quad (1)$$

where $\hat{\rho}_q$ is the LLL projected density operator, q is the complex coordinate of momentum, which is $q = (q_x + iq_y)/\sqrt{2}$ in an isotropic LL, and l_B is the magnetic length. The density operator deforms the shape of LLs while preserving their LL index [12–15]. The GMP algebra is important for FQH physics in many aspects, including the conformal field theory mapping [16,17], constructing exact pseudopotential projectors that protect the stability of FQH states [18,19], and others. The GMP algebra was initially derived based on the holomorphicity of LLL wave functions [20], which arises from the noncommutativity of guiding centers and in fact applies to any LL [21].

Topological flatbands realized in lattice systems are more complicated than LLs. They can carry an arbitrary integer Chern number, and typically do not exhibit uniform Berry

*jjewang.phy@gmail.com

†zhaol@zju.edu.cn

Published by the American Physical Society under the terms of the [Creative Commons Attribution 4.0 International](https://creativecommons.org/licenses/by/4.0/) license. Further distribution of this work must maintain attribution to the author(s) and the published article's title, journal citation, and DOI.

curvature. Due to this complication, neither the holomorphicity of the wave function nor the exact projected density algebra exist, thereby Eq. (1) becomes approximate. As a consequence, FCIs are no longer expected to be exact, and their stability is supposed to be reduced [22]. There have been important attempts towards restoring the GMP algebra in flatband systems. For instance, Ref. [23] highlighted the importance of the Fubini-Study metric g_k^{ab} , which is the intrinsic wave-function distance measure. Given constant Berry curvature $\Omega_k = \Omega$ and the so-called trace condition $\text{Tr}g_k = \Omega_k$, Ref. [23] derived a GMP algebra for all topological flatbands of $\mathcal{C} \neq 0$. However, the assumption of constant Berry curvature oversimplified the flatband problem.

In this work, we relax the above assumption by focusing on ideal flatbands satisfying the following conditions [24]:

$$g_k^{ab} = \frac{1}{2}\omega^{ab}\Omega_k, \quad \Omega_k > 0 \quad \text{for } \forall \mathbf{k}. \quad (2)$$

The ω_{ab} is a constant unimodular matrix. The Berry curvature is assumed to be positive-definite but not necessarily uniform. Recently, it was shown that Eq. (2) is necessarily [25] and sufficiently [26–28] equivalent to the momentum-space holomorphicity, which is a key geometric property of the momentum-space (= boundary-condition space). For all $\mathcal{C} = 1$ ideal flatbands such as those realized in the chiral model of twisted bilayer graphene [29,30] and others [31–33], it has been shown that momentum-space holomorphicity highly constrains the wave function to admit a universal form descending from the LLL wave function [24]. Such simplicity enables exact construction of many-body model wave functions [30] as well as exact projective pseudopotential Hamiltonians [24], hence the ideal condition plays an important role in experimental realization and identification of FCIs [34,35]. Recently the ideal condition Eq. (2) has been generalized to a larger family called “vortexability” [36] by allowing nonlinear real-space embedding [37].

While much progress has been made for $\mathcal{C} = 1$, less is known for generic cases of $\mathcal{C} > 1$. Recently, solvable models based on twisted multilayer graphene sheets were proposed that realize ideal flatbands of arbitrary Chern number [38,39]. Remarkably, exact Halperin-type FCIs were found by numerical diagonalization [38]. Motivated by the $\mathcal{C} = 1$ case, it was conjectured that the momentum-space holomorphicity is also the fundamental reason for their emergence [38], however the nature of the Bloch wave function and why FCIs are stable are still far from being thoroughly understood.

In this work, we prove that the ideal quantum geometric condition, without assuming the flatness of Ω_k or g_k themselves, is sufficient to guarantee exact GMP algebra and model FCI states occurring as exact zero-energy ground states of proper short-ranged interactions in all $\mathcal{C} \geq 1$ ideal flatbands. We achieve these results by pointing out the importance of an emergent Hilbert space in which the wave functions’ normalization factors are adjusted to flatten Berry curvature in an exact manner. Importantly, this leads to a simple algebra for the projected coordinates identical to the guiding center algebra in LLs, and it enables an exact derivation for the single-particle wave function in ideal flatbands. The general form Bloch wave function is found to be a nonlinear superposition of LLL wave functions of \mathcal{C} distinct boundary conditions, generalizing the previously proposed

color-entangled wave functions with uniform Berry curvature [40–42] to the case of fluctuating Berry curvature. The density algebra is proved to be closed, extending the GMP algebra initially derived for $\mathcal{C} = 1$ LLs to generic $\mathcal{C} \geq 1$ ideal flatbands. The closeness of the density algebra leads directly to the exact FCIs stabilized by generic M -body repulsive interactions which are Halperin-type when $\mathcal{C} > 1$ and typically non-Abelian when $M > 2$. Thus the ideal condition Eq. (2) provides a general and exact statement for stabilizing FCIs regardless of the nonuniformness of Berry curvature.

The paper is structured as follows. In Sec. II, we pose the problem by showing unusual numerical observations. In Sec. III, we review key analytical results for ideal flatbands, emphasizing their real and momentum-space boundary conditions, and we define the emergent Hilbert space. We show in Sec. IV a well-defined guiding center in the ideal flatband problems, which leads to the derivation of single-particle wave functions in Sec. V. In Sec. VI, the density algebra is derived, and the origin of model FCIs is explained. We discuss application of the theory to FCIs and symmetry-breaking phases [34,43] in moiré flatband systems in Sec. VII.

II. MOTIVATION FROM UNUSUAL NUMERICAL OBSERVATIONS

The ideal flatbands are not abstract concepts, rather they can be realized in concrete models including Dirac fermion based models [29,33,38,39] and Kapit-Mueller models [31,32,44,45]. In particular, in chiral twisted multilayer graphene models [38,39], ideal flatbands of arbitrary $\mathcal{C} \neq 0$ are realized exactly. In this section, we use this model as a concrete platform to numerically study the interacting spectra, which point out a couple of important and unusual aspects of the projected density operator that motivates the theory to be discussed in the following sections.

For self-consistency, we first briefly review the chiral twisted multilayer graphene models [38,39], although the model details are not crucial for the current discussion. Details about the chiral twisted graphene model and beyond can be found in the literature [29,30,46–51]. The chiral twisted multilayer model consists of two sheets of graphene multilayers each of which has n layers and is A/B stacked without twist [52–54]. The top sheets are twisted relative to the bottom sheets as a whole by a twist angle θ . See Fig. 1(a) for illustration of the setup. At magic twist angles, the model exhibits two exactly dispersionless degenerate bands shown in Fig. 1(b), which have Chern number $\mathcal{C} = \pm n$. Such degeneracy can be easily lifted by a sublattice contrasting potential, and we focus on the $\mathcal{C} = n$ band. The flatband wave function is derived in Refs. [38,39], and its components on the outmost layers are found to be responsible for the high Chern number and zero-mode FCIs. We hence project the wave function to the outmost layers to get an effective single-component wave function, denoted as $\phi_k^{\text{Bloch}}(\mathbf{r})$. It can be numerically verified that $\phi_k^{\text{Bloch}}(\mathbf{r})$ is smooth in both \mathbf{k} and \mathbf{r} . The Berry curvature associated with $\phi_k^{\text{Bloch}}(\mathbf{r})$, defined through the standard definition,

$$\Omega_k = \epsilon_{ab}\partial_k^a A_k^b, \quad A_k^a \equiv -i\langle u_k^{\text{Bloch}} | \partial_k^a u_k^{\text{Bloch}} \rangle, \quad (3)$$

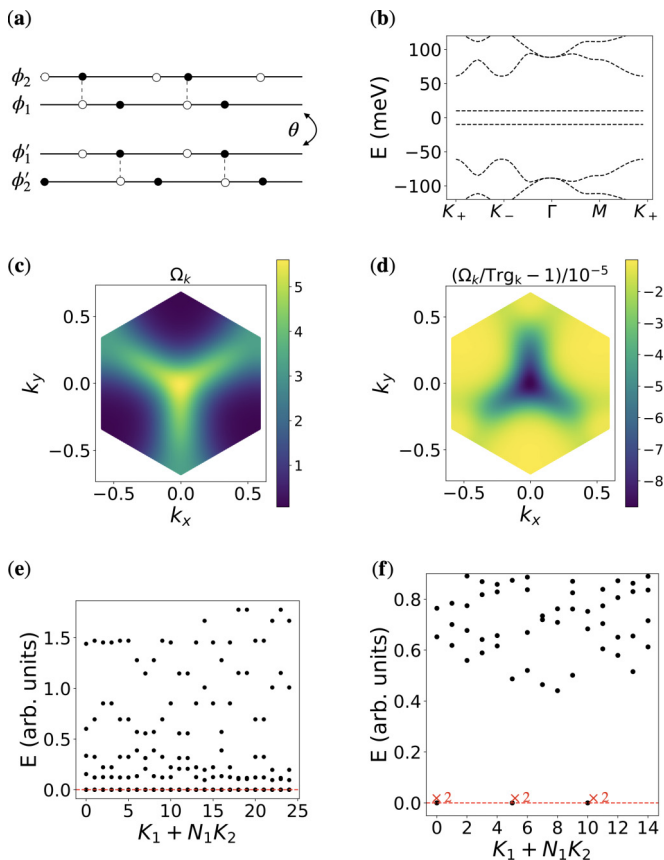


FIG. 1. (a) Illustration of the chiral twisted multilayered graphene model, where solid and empty dots represent the A and B sublattice, respectively, and the interlayer tunneling is assumed to be chiral and represented by the dashed line. The $\phi_{1,\dots,n}$ and $\phi'_{1,\dots,n}$ label the layer component. (b) The band structure where a tiny sublattice bias potential is used to split the twofold degeneracy of the flatbands. The resulting two bands are entirely sublattice-polarized. (c) and (d) The Berry curvature and the trace condition of u_k^{Bloch} defined in the main text. The Berry curvature is positive-definite. (e) The energy spectrum of the two-body $v_{m=1}$ interaction for two fermions on an $N_1 \times N_2 = 5 \times 5$ lattice. At each momentum \mathbf{k} , there are precisely $(m+1)\mathcal{C} = 4$ nonzero eigenvalues. (f) The energy spectrum of the three-body on-site interaction for $N = 10$ bosons on an $N_1 \times N_2 = 5 \times 3$ lattice. The exact sixfold-degenerate zero-energy ground states are non-Abelian model FCIs that are analogous to the FQH non-Abelian spin-singlet state (NASS). In (a)–(f) we use $n = 2$, namely the twisted double bilayer graphene model, as an example.

is plotted in Fig. 1(c), which integrates to the Chern number $\mathcal{C} = n$. Here $u_k^{\text{Bloch}}(\mathbf{r}) = e^{-i\mathbf{k}\cdot\mathbf{r}}\phi_k^{\text{Bloch}}(\mathbf{r})$ is the cell-periodic part of the Bloch wave function. Its ideal geometry condition can be either analytically proved or numerically verified to be satisfied [38,39]. See Fig. 1(d) for the plot of the trace condition for the $n = 2$ model where errors are finite-size artifacts that will vanish in the infinite-size limit.

We then consider interacting phenomena when the flatband is partially filled. We focus on finite systems on the torus geometry at band filling, $\nu = N/(N_1N_2)$, where N is the number of particles and $N_{1,2}$ is the number of unit cells in each primitive direction of the lattice. The two-body density-density

interaction takes the form

$$H = \sum_{\mathbf{q}} v(\mathbf{q}) : \hat{\rho}_{\mathbf{q}} \hat{\rho}_{-\mathbf{q}} :, \quad (4)$$

where $v(\mathbf{q})$ is the Fourier transform of the interaction potential, $\hat{\rho}_{\mathbf{q}}$ is the band-projected density operator, and $::$ is the normal ordering. Because of the translation invariance by lattice vectors, the energy spectrum of H can be resolved by the center-of-mass momentum (K_1, K_2) . We are particularly interested in the repulsive interaction $v_m(\mathbf{r}_1 - \mathbf{r}_2) = \sum_{\mathbf{q}} v_m(\mathbf{q}) e^{i\mathbf{q}\cdot(\mathbf{r}_1 - \mathbf{r}_2)}$, whose Fourier transform $v_m(\mathbf{q})$ has a series expansion of order no higher than m :

$$v_m(\mathbf{q}) = c_0 + c_1|\mathbf{q}|^2 + c_2|\mathbf{q}|^4 + \dots + c_m|\mathbf{q}|^{2m}. \quad (5)$$

The above series expansion is equivalent to an interaction range expansion, as the real space form of the $|\mathbf{q}|^{2n}$ term is given by the $2n$ th derivative of the contact interaction $\delta(\mathbf{r}_1 - \mathbf{r}_2)$. In particular, v_0 and v_1 are the shortest interactions for bosons and fermions, respectively [55].

We first consider two particles interacting with v_m , where m is even for bosons and odd for fermions. While it is unrealistic for bosons to occupy the flatband near charge neutrality of twisted double bilayer graphene, we can still use that setup to examine the band property. Remarkably, for any choice of m and Chern number \mathcal{C} , the two-particle spectrum always shows a dispersive “band” with a fixed number of nonzero eigenvalues at each momentum \mathbf{k} , no matter what the lattice size is. The dimension of this finite-energy “band” is precisely $(m+1)\mathcal{C}$ for fermions and $(m+1)\mathcal{C} + 1$ for bosons. The same counting is expected in the two-particle problem in a \mathcal{C} ideal flatband exhibits intrinsic \mathcal{C} internal degree of freedom playing the role of \mathcal{C} layers [56]. Moreover, the “band” dispersion of the two-particle spectrum reflects the fact that Berry curvature is nonuniform. Apart from these finite-energy levels, there are also massive zero modes whose dimension increases with the system size. The typical example with $m = 1$, $\mathcal{C} = 2$ is demonstrated in Fig. 1(e) for two fermions. Such two-particle spectra are different from those in either LLs or generic flatbands. For generic flatbands without ideal geometry, the zero modes would not appear and the dimension of finite-energy levels is hence lattice-size-dependent [5,57]. In a LL, as the v_m interaction only picks out two-particle coherent states of relative angular momentum no greater than m , both a finite-energy band whose dimension is independent of the system size and massive zero modes appear, however the “band” is nondispersive due to the continuous translation symmetry. Therefore, Fig. 1(e) clearly shows there is an emergent projector property associated with the density operator of ideal flatbands, which, however, unlike in LLs, is influenced by the nonuniform Berry curvature.

We can further generalize Eq. (4) to multibody interactions. In Fig. 1(f), the spectrum of the three-body on-site interaction is plotted for bosons at $\nu = 2/3$ in the $\mathcal{C} = 2$ band. In this case, a sixfold exact ground-state degeneracy at zero energy is obtained. These zero modes are expected to be lattice analogs of the non-Abelian spin singlet states, which are generalizations of the Abelian Halperin topological order in bilayer LLL [58]. This result indicates that suitable short-range M -body repulsions can stabilize model FCIs of both

Abelian and non-Abelian types in high Chern number ideal flatbands. Moreover, it points out that two-body interaction is not special: there should be a general property that the projected density operator obeys in order to give rise to FCIs stabilized by generic M -body interactions [59].

To summarize, numerical studies on interacting two-particle spectra and three-body interactions point out the importance of the flatband projected density operator, which exhibits emergent projector properties and internal \mathcal{C} degrees of freedom playing the role of layers, although the underlying Berry curvature can be highly nonuniform. It motivates the following two questions:

(i) What internal degrees of freedom in the scalar-valued wave function $u_k(\mathbf{r})$ play the role of layers?

(ii) Why does the nonuniform Berry curvature not destabilize the Abelian and non-Abelian FCIs (i.e., why are exact many-body zero modes preserved even in the presence of nonuniform Berry curvature)?

Thorough this work, we will show the answers to these two questions by deriving the general form of $\mathcal{C} \neq 0$ ideal flatband wave functions, illustrating their physical meanings and studying their density algebra, which we find generalizes the GMP algebra Eq. (1) in a nontrivial way.

III. ANALYTICAL PROPERTIES OF IDEAL FLATBANDS

As we have shown, numerical experiments in ideal flatbands point out the unusual effects of ideal quantum geometry on interacting problems. To address the two questions at the end of the last section, we will focus on analytical derivations in the remaining parts of this article. We start with reviewing the ideal quantum geometric condition and emphasizing its relation to the momentum-space Kähler condition in this section. The momentum-space Kähler condition gives novel properties of the Bloch wave function in many aspects, such as the unique boundary condition and the relation between Berry curvature and the normalization factor. These general results were derived for ideal flatbands in Ref. [24]. In Sec. IV, we will discuss results about their important implication for the well-defined guiding center, which establishes a connection to LL physics in the presence of nonuniform Berry curvature.

A. Ideal quantum geometry and Kähler geometry

First of all, we set up conventions in more detail. Our exact results apply to arbitrary system size $N_{1,2}$. The system is spanned by primitive lattice vectors $\mathbf{a}_{1,2}$ containing an area $|\mathbf{a}_1 \times \mathbf{a}_2| = 2\pi S$, and throughout this work we set $S = 1$ as the unit area scale. The reciprocal/momentum space is spanned by reciprocal-lattice vectors \mathbf{b}_i such that $\mathbf{a}_i \cdot \mathbf{b}_j = 2\pi \delta_{ij}$ is satisfied.

We consider a single-component complex-valued Bloch wave function defined on this torus. Its cell periodic part $u_k^{\text{Bloch}}(\mathbf{r})$ is lattice translational invariant following the Bloch theorem $u_k^{\text{Bloch}}(\mathbf{r}) = u_k^{\text{Bloch}}(\mathbf{r} + \mathbf{a})$ for arbitrary lattice vectors $\mathbf{a} = m_1 \mathbf{a}_1 + m_2 \mathbf{a}_2$ and $m_{1,2} \in \mathbb{Z}$. The $u_k^{\text{Bloch}}(\mathbf{r})$ is assumed to be smooth in both \mathbf{k} and \mathbf{r} . Momentum quantization restricts $\mathbf{k} = (n_1/N_1 + \phi_1/2\pi)\mathbf{b}_1 + (n_2/N_2 + \phi_2/2\pi)\mathbf{b}_2$, where $n_{1,2} \in \mathbb{Z}$ and $\phi_{1,2}$ are fictitious boundary condition fluxes. Our result applies to arbitrary $\phi_{1,2}$ too, so without loss of generality

we set $\phi_{1,2} = 0$. Because the flux space (a torus formed by continuous variable $\phi_{1,2}$) is equivalent to the momentum space in the presence of translational symmetry, we use these two spaces interchangeably. The discussions in this work can be generalized to flux space for systems without translation symmetry where the notion of momentum is not defined.

$u_k^{\text{Bloch}}(\mathbf{r})$ satisfies the ideal quantum geometric condition while not necessarily carrying flat Berry curvature. We assume u_k^{Bloch} has a positive Chern number; a negative Chern number is a simple generalization. Because it is a positive integer, the Chern number can be factorized into two positive integers $\mathcal{C} = \mathcal{C}_1 \mathcal{C}_2$, and the factorization, as we will discuss, is a gauge choice.

Systematic studies of flatbands with momentum-space holomorphicity start from Refs. [25,60], where the authors found that the ideal condition is automatically satisfied if the cell-periodic part of the Bloch wave function $u_k^{\text{Bloch}}(\mathbf{r})$ is given by Eq. (6). Very recently, Refs. [26–28] pointed out that the inverse is also true: the ideal condition generally implies that u_k^{Bloch} can be written as Eq. (6) under a gauge choice up to a positive-definite normalization factor N_k :

$$u_k^{\text{Bloch}}(\mathbf{r}) = N_k u_k^{\text{holo}}(\mathbf{r}), \quad \bar{\partial}_k u_k^{\text{holo}} = 0, \quad (6)$$

where the holomorphic coordinate k (the unbold letter) is defined as $k \equiv \omega^a \mathbf{k}_a$, and the associated antiholomorphic derivative is defined as $\bar{\partial}_k \equiv \omega_a \partial_k^a$. Technically, the notion of holomorphicity ω^a is defined from factorizing the constant unimodular matrix ω^{ab} and the antisymmetric tensor ϵ^{ab} as follows [21]:

$$\begin{aligned} \omega^{ab} &= \omega^a \omega^{b*} + \omega^{a*} \omega^b, \\ i\epsilon^{ab} &= \omega^{a*} \omega^b - \omega^a \omega^{b*}. \end{aligned} \quad (7)$$

The vectors satisfy $\omega^{a*} \omega_a = 1$, $\omega^a \omega_a = 0$; throughout the paper, Einstein summation is implicitly assumed, and their indices are raised or lowered by ω^{ab} . Note that in the isotropic case $(\omega^x, \omega^y) = (1, i)/\sqrt{2}$ the complex coordinate reduces to the conventional form $k = (k_x + ik_y)/\sqrt{2}$. We will work in the general case without assuming isotropy.

It is worth mentioning that ω^a has an equivalent canonical definition as it is the constant null vector of the quantum geometric tensor [24]:

$$Q_k^{ab} \omega_b = 0 \quad \text{for } \forall k, \quad (8)$$

where the quantum geometric tensor is defined by using the covariant derivative of wave functions $D_k^a = \partial_k^a - iA_k^a$, where the Berry connection A_k^a is found in Eq. (3), whose real symmetric and imaginary antisymmetric parts are the Fubini-Study metric and the Berry curvature, respectively:

$$Q_k^{ab} \equiv \langle D_k^a u_k^{\text{Bloch}} | D_k^b u_k^{\text{Bloch}} \rangle = g_k^{ab} + i \frac{\epsilon^{ab}}{2} \Omega_k. \quad (9)$$

B. Implications from Kähler geometry

We have reviewed the relation between the ideal quantum geometric condition and momentum-space holomorphicity [25–28]. In this section, we discuss two implications from Kähler geometry: the uniqueness of the boundary condition, and the relation between the normalization factor and Berry

curvature. They are important in deriving the ideal flatband wave function and the density algebra.

1. Uniqueness of the boundary condition $\phi_{k,b}$

Following Ref. [24], we can generally denote the momentum-space boundary condition of u_k^{holo} as

$$u_{k+b_i}^{\text{holo}}(\mathbf{r}) = u_k^{\text{holo}}(\mathbf{r}) \exp(-i\mathbf{b}_i \cdot \mathbf{r} + i\phi_{k,b_i}), \quad (10)$$

where the complex phase $\phi_{k,b}$ is not only required to be holomorphic in k but is also constrained to satisfy a cocycle relation [24],

$$-2\pi\mathcal{C} = \phi_{b_1,b_2} - \phi_{0,b_2} + \phi_{0,b_1} - \phi_{b_2,b_1}. \quad (11)$$

Such a constraint [Eq. (11)] is required from the simplified Chern number formula derived for ideal flatbands [24]:

$$\mathcal{C} = \frac{1}{2\pi i} \oint dk \partial_k \ln u_k^{\text{holo}}(\mathbf{r}), \quad (12)$$

which means that the winding of the wave function in the momentum space around the Brillouin zone at any fixed \mathbf{r} must reflect the topology of the wave function. The cocycle relation Eq. (11) implies that the boundary condition factor $\phi_{k,b}$ must be a linear function of holomorphic coordinate k [24]. The phase $\phi_{k,b}$ is the so-called factor of automorphy which appears in classifying holomorphic line bundles [61]. Following the results of holomorphic line bundle classification, the boundary condition complex phase $\phi_{k,b}$ is unique up to gauge transformations [61]. Without loss of generality, we choose the symmetric gauge,

$$\phi_{k,b_j} = \mathcal{C}b_j^*(-ik - ib_j/2) + \mathcal{C}_j\pi, \quad j = 1, 2, \quad (13)$$

where $\mathcal{C}_{1,2}$ are the two positive integers dividing the Chern number $\mathcal{C} = \mathcal{C}_1\mathcal{C}_2$, and the ambiguity in their choice will prove to be unimportant.

2. Kähler potential

The antiholomorphic component of the Berry connection $\bar{A}_k \equiv \omega_a A_k^a$ can be computed from the standard definition:

$$\begin{aligned} \bar{A}_k &\equiv -i\langle u_k^{\text{Bloch}} | \bar{\partial}_k u_k^{\text{Bloch}} \rangle, \\ &= -i \int d^2\mathbf{r} N_k u_k^{\text{holo}*}(\mathbf{r}) \bar{\partial}_k [N_k u_k^{\text{holo}}(\mathbf{r})], \\ &= -i(N_k^{-1} \bar{\partial}_k N_k) \int d^2\mathbf{r} N_k^2 u_k^{\text{holo}*}(\mathbf{r}) u_k^{\text{holo}}(\mathbf{r}), \\ &= -i \bar{\partial}_k \ln N_k. \end{aligned} \quad (14)$$

Then from $\Omega_k = -i(\partial_k \bar{A}_k - \bar{\partial}_k A_k)$, where A_k is the complex-conjugate of \bar{A}_k , we obtain the expression for the Berry curvature [24,62,63]:

$$\Omega_k = -2\partial_k \bar{\partial}_k \ln N_k. \quad (15)$$

Equation (15) shows that $\ln N_k$ is the momentum-space Kähler potential that governs the spatial fluctuation of Berry curvature. It has an important implication: for ideal flatbands, the Berry curvature can be effectively flattened by adjusted by the normalization of the wave function. More precisely, by factorizing N_k into

$$N_k = e^{-\frac{\mathcal{C}}{4}|k|^2} \tilde{N}_k, \quad (16)$$

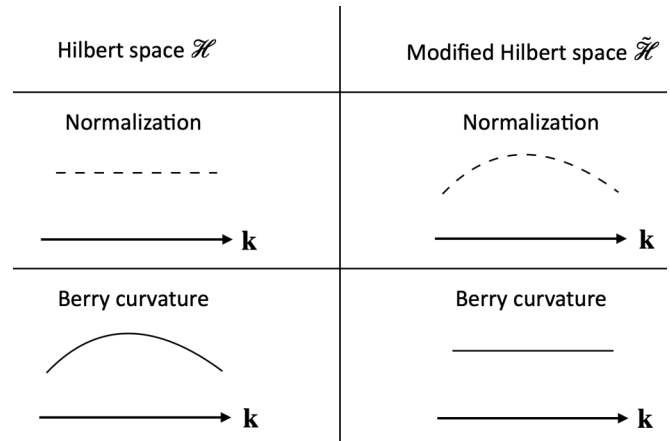


FIG. 2. The normalized flatband wave function defines a Hilbert space \mathcal{H} where the Berry curvature is nonuniform. For ideal flatbands, the wave function’s normalization can be tuned such that the resulting wave function $u_k(\mathbf{r})$ defines a modified Hilbert space $\tilde{\mathcal{H}}$ in which Berry curvature can be exactly flattened. As a consequence, $u_k \in \tilde{\mathcal{H}}$ perceives an identical k -dependence as LLL wave functions. Such a property greatly simplifies the problem, enabling a thorough characterization of a flatband wave function from a momentum-space formulation. As an illustration, we used \mathbf{k} to represent the 2D momentum-space. The normalization and Berry curvature are represented by the dashed and solid lines, respectively.

the Berry curvature is accordingly split into $\Omega_k = \mathcal{C} + \tilde{\Omega}_k$, i.e., the uniform and fluctuating parts. The fluctuating part $\tilde{\Omega}_k = -2\partial_k \bar{\partial}_k \ln \tilde{N}_k$ averages to zero when being integrated over the Brillouin zone, which does not contribute to the quantization.

We can thus flatten the Berry curvature by adjusting the normalization of the wave function. See Fig. 2 for an illustration. We define the following unnormalized wave function $u_k(\mathbf{r})$, which perceives constant Berry curvature, to be in the modified Hilbert space $\tilde{\mathcal{H}}$ [64]:

$$u_k(\mathbf{r}) \equiv \tilde{N}_k^{-1} u_k^{\text{Bloch}}(\mathbf{r}) = e^{-\frac{\mathcal{C}}{4}k^2} u_k^{\text{holo}}(\mathbf{r}). \quad (17)$$

An important consequence is that u_k perceives a flattened Berry curvature and has the same k -dependence as the LLL wave functions. Therefore, the momentum-space formulation of the LLL problem can be directly applied to flatband problems, which we will discuss in detail in the following section.

To summarize, in this section we reviewed two implications from Kähler geometry: the uniqueness of the boundary condition and the relation between normalization and Berry curvature. We use the latter to define a modified Hilbert space $\tilde{\mathcal{H}}$ in which the wave functions $u_k(\mathbf{r})$ perceive constant Berry curvature. We summarize the real-space and boundary-condition space of $u_k(\mathbf{r})$ below by combining results from Eqs. (10), (13), and (17) [65]:

$$u_k(\mathbf{r} + \mathbf{a}_i) = u_k(\mathbf{r}), \quad (18)$$

$$e^{-\frac{i\mathcal{C}}{2}b_i \times k} u_{k+b_i}(\mathbf{r}) = (-1)^{C_i} e^{-i\mathbf{b}_i \cdot \mathbf{r}} u_k(\mathbf{r}). \quad (19)$$

In Sec. V, we will use these boundary conditions to determine the most general form of $u_k(\mathbf{r})$. In the next section, we discuss the guiding centers in ideal flatbands and point out their sim-

ple algebra in $\hat{\mathcal{H}}$, which is essential to many aspects of ideal flatbands.

IV. GUIDING CENTER IN IDEAL FLATBANDS

The guiding centers are particles' projected coordinates, which typically are noncommutative. They and their algebra are known to play a crucial role in quantum Hall physics. In this section, we first review guiding center in LLs, followed by discussing the difficulty faced by generic flatbands. In the end, we show that the ideal flatbands are exceptions, because there are well-defined guiding centers with closed simple algebra.

A. Guiding center in Landau levels

In LLs, an electron's coordinate is split into the guiding center \hat{R} and Landau orbital \hat{R} which correspond to the center and cyclotron motion of classical orbitals, respectively. Without loss of generality, we choose a symmetric gauge under which the guiding center and Landau orbital are

$$\hat{R}^a = -il_B^2 \epsilon^{ab} \partial_b + r^a/2, \quad (20)$$

$$\hat{R}^a = +il_B^2 \epsilon^{ab} \partial_b + r^a/2. \quad (21)$$

They form two independent sets of Heisenberg algebras $[\hat{R}^a, \hat{R}^b] = 0$,

$$[\hat{R}^a, \hat{R}^b] = -il_B^2 \epsilon^{ab} \quad (22)$$

and $[\hat{R}^a, \hat{R}^b] = +il_B^2 \epsilon^{ab}$. In particular, Eq. (22) can be called "guiding center algebra."

The guiding centers and their algebra are one of the most important intrinsic features for physics inside a single LL [21]. They are the essence of many "ideal aspects" of Landau levels: for instance, they are the physical origin of the holomorphicity of LLs [21], they imply an infinite degree of deformation symmetry [12,13], and they are crucial to the stability of FQH states [16,18].

A physically intuitive way to think of Eq. (22) is based on the coherent state: the projected particle is no longer a point particle but has finite support, and Eq. (22) describes the uncertainty of its 2D coordinates. Such a coherent state can be translated or deformed while preserving the area, and in fact these processes are all generated by operations constructed from guiding centers. More precisely, the \hat{R} itself is the generator of a magnetic translation group, and $\hat{\Lambda}^{ab} = \{\hat{R}^a, \hat{R}^b\}/2$ deforms the metric of the coherent state while preserving its determinant, and in fact such metric deformation gives a Hall viscosity response [21,66–68]. Most generally, all area-preserving deformation of Landau levels is generated by $e^{iq \cdot \hat{R}}$, whose leading- and second-order expansion in q correspond to the magnetic translation and metric deformation, respectively, and generally all higher-order deformations exist. Due to the simple form of the guiding center algebra, Eq. (22), it is straightforward to derive the algebra for $e^{iq \cdot \hat{R}}$:

$$[e^{iq_1 \cdot \hat{R}}, e^{iq_2 \cdot \hat{R}}] = 2i \sin\left(\frac{\mathbf{q}_1 \times \mathbf{q}_2}{2} l_B^2\right) e^{i(q_1+q_2) \cdot \hat{R}}, \quad (23)$$

which in fact is precisely equivalent to the GMP algebra shown in Eq. (1) when noticing that the LLL projected density

operator is $\hat{\rho}_q = e^{iq \cdot \hat{R}} e^{-\frac{1}{4} q^2 l_B^2}$, where the Gaussian factor is the form factor.

B. Why GMP algebra fails in generic flatbands

Following Blount [25,69–71], the projected coordinates \hat{r} are given below for band systems:

$$\begin{aligned} \hat{Q}_{\text{Bloch}}^a &\equiv -i\partial_k^a - \langle u_k^{\text{Bloch}} | i\partial_k^a u_k^{\text{Bloch}} \rangle, \\ &= -i\partial_k^a + A_k^a. \end{aligned} \quad (24)$$

To avoid the real-space representation as used for LLs, we denote the above k -space representation as \hat{Q} . It is straightforward to check that their commutator is the Berry curvature 2 form,

$$\begin{aligned} [\hat{Q}_{\text{Bloch}}^a, \hat{Q}_{\text{Bloch}}^b] &= -i\partial_k^a A_k^b - (a \leftrightarrow b), \\ &= -i\epsilon^{ab} \Omega_k. \end{aligned} \quad (25)$$

This immediately means that higher-order commutators such as $[\hat{Q}_{\text{Bloch}}^a, [\hat{Q}_{\text{Bloch}}^b, \hat{Q}_{\text{Bloch}}^c]]$ depend on the Berry curvature derivative $\partial_k^a \Omega_k$, which generally is nonvanishing in flatband systems. As a consequence, the GMP algebra is *not* expected to exist, reducing the stability of correlated phases of matter due to such geometric instability [22,72,73].

C. Emergent guiding center algebra in ideal flatbands

In this section, we point out the exact and extremely simple guiding center algebra that emerges in ideal flatbands. The key reason lies in the Kähler potential discussed in Sec. III B 2. It means that the complication from the nonuniform part of Berry curvature can be exactly and completely removed by adjusting the normalization of the Bloch wave function.

The \mathcal{H} -space projected coordinate operator is

$$\begin{aligned} \hat{Q}^a &\equiv -i\partial_k^a - \langle u_k | i\partial_k^a u_k \rangle \\ &= -i\partial_k^a - C\epsilon^{ab} k_b/2. \end{aligned} \quad (26)$$

Equation (26) is derived as follows: we can first look at $\omega_a \hat{Q}^a$; following the definition of projected coordinates Eq. (24) and wave function Eq. (17), we have

$$\begin{aligned} \omega_a \hat{Q}^a &= -i\bar{\partial}_k - \langle u_k | i\bar{\partial}_k u_k \rangle \\ &= -i\bar{\partial}_k + iCk/2, \end{aligned} \quad (27)$$

which immediately implies Eq. (26), because \hat{Q}^a is the linear combination of $\omega_a \hat{Q}^a$ and its complex conjugate. Technically we have treated $u_k(\mathbf{r})$ as normalized wave functions when computing the expectation value of any operator \hat{O} in this way, $O_{kk'} \equiv \int d^2\mathbf{r} u_k^*(\mathbf{r}) O(\mathbf{r}) u_{k'}(\mathbf{r})$, without dividing their normalization $\tilde{N}_k \tilde{N}_{k'}$.

Interestingly, Eq. (26) takes a similar form to the guiding center of LLs [Eq. (20)] but formulated in momentum space and using an effective magnetic length $l_B^2 = C$. In analogy to the Landau orbital operator in LLs, we define the following operator:

$$\hat{Q}^a \equiv -i\partial_k^a + C\epsilon^{ab} k_b/2, \quad (28)$$

which commutes with \hat{Q}^a . It is easy to check that \hat{Q} and $\hat{\hat{Q}}$ individually obey the Heisenberg algebra:

$$[\hat{Q}^a, \hat{Q}^b] = -i\epsilon^{ab}\mathcal{C}, \quad (29)$$

$$[\hat{\hat{Q}}^a, \hat{\hat{Q}}^b] = +i\epsilon^{ab}\mathcal{C}. \quad (30)$$

\hat{Q} and $\hat{\hat{Q}}$ are in fact the momentum-space form of the guiding center and the Landau orbital, respectively. For this reason, we can refer to them as the dual guiding center and the dual Landau orbital. The existence of two such well-defined sets of Heisenberg algebra is important to the physics in ideal flatbands. For instance, in the so-called ‘‘LLL condition,’’ i.e., the magnetic translation algebra, pseudopotentials are all well defined in an exact manner for ideal flatbands, but generalized from LLs in a nontrivial way. We illustrate their meaning one by one throughout this paper. To begin with, we discuss the ‘‘dual LLL condition,’’ which is seen from noticing that the modified Hilbert space $\tilde{\mathcal{H}}$ is completely annihilated by the following ladder operator analogous to the Landau level annihilation operator used in quantum Hall physics:

$$\hat{a}u_k = 0, \quad \forall u_k \in \tilde{\mathcal{H}}, \quad (31)$$

where

$$\hat{a} \equiv \omega_a \hat{Q}^a = -i\partial_k + iC\bar{k}/2. \quad (32)$$

Moreover, the dual guiding center \hat{Q} leaves the Hilbert space $\tilde{\mathcal{H}}$ invariant, because it commutes with \hat{Q} . Then there exists another set of ladder operators,

$$\hat{a} \equiv \omega_a^* \hat{Q}^a / \sqrt{\mathcal{C}}, \quad \hat{a}^\dagger \equiv \omega_a \hat{Q}^a / \sqrt{\mathcal{C}}, \quad [\hat{a}, \hat{a}^\dagger] = 1, \quad (33)$$

such that they map states within $\tilde{\mathcal{H}}$:

$$\hat{a}u_k \in \tilde{\mathcal{H}}, \quad \hat{a}^\dagger u_k \in \tilde{\mathcal{H}}, \quad \forall u_k \in \tilde{\mathcal{H}}. \quad (34)$$

In this sense, $\tilde{\mathcal{H}}$ behaves like the LLL Hilbert space in quantum Hall physics, and hence we expect that u_k will show similarity in its form with the LLL wave function. In the next section, we utilize such properties to fully characterize the ideal flatband wave function, following the same idea of how the torus quantum Hall wave function was initially derived [74,75].

We comment that the choice of gauges, i.e., the Brillouin zone factorization $\mathcal{C}_{1,2}$ and the particular form of $\phi_{k,b}$, only affects the concrete form of dual guiding centers and dual Landau orbitals. For ideal flatbands, the existence of such a complete separation of two sets of Heisenberg algebras is a fundamental consequence of ideal quantum geometry and is gauge-independent. This is also the key for the existence of exact properties even in the presence of nontrivial Berry curvature.

To summarize this section, the flattening of Berry curvature in the modified Hilbert space $\tilde{\mathcal{H}}$ greatly simplifies the ideal flatband problem. The $\tilde{\mathcal{H}}$ -space projected coordinates, i.e., the dual guiding centers, map states within $\tilde{\mathcal{H}}$ and obey the same algebra as the guiding centers in LLs. Therefore, tools from quantum Hall physics can be applied to analyze ideal flatbands in many aspects, which we discuss in the following sections.

V. IDEAL FLATBAND WAVE FUNCTION

The emergence of guiding centers and their exact algebra in ideal flatbands can greatly simplify the flatband problem while retaining their nontrivial aspect: nonuniform quantum geometries. It also motivates the idea that tools from quantum Hall physics can be applied to analyze the flatband problem. In this section, we point out that it is crucial to adopt a position-momentum exchanged view to carefully compare the two systems: ideal flatband and Landau levels [25]. Importantly, we point out that the wave functions of ideal flatbands are highly constrained by their quantum geometry, exactly how the LLL wave function is highly constrained by the magnetic field [74,75]. Utilizing the emergent dual guiding centers and their algebra, we define a dual version of the magnetic translation group and use it to fully characterize the ideal flatband wave function. We prove that there is a unique general form of the single-particle Bloch wave function for all topological ideal flatbands, and we provide their explicit first quantized expression.

A. Dual magnetic translation group

In Landau levels, the guiding center \hat{R} generates the magnetic translation group (MTG), which adiabatically transports particles while preserving them within the LL where they initially started. In this section, we define the dual-MTG for ideal flatbands, such that this group adiabatically transports Bloch wave functions while preserving their ideal quantum geometric condition. We then use the dual-MTG to derive ideal flatband wave functions.

The dual-MTG is generated by the dual guiding centers. Its group elements are

$$t(\mathbf{q}) = e^{i\mathbf{q}\hat{Q}} = e^{-\frac{i\mathcal{C}}{2}\mathbf{q}\times\mathbf{k}} e^{q\cdot\partial_k}. \quad (35)$$

As discussed in the last section, the dual guiding center leaves $\tilde{\mathcal{H}}$ invariant. Therefore, $t(\mathbf{q})$ also maps states within $\tilde{\mathcal{H}}$ and preserves their ideal quantum geometric condition. The algebra of the dual-MTG is easily derived based on the noncommutativity of \hat{Q} :

$$t(\mathbf{q}_1)t(\mathbf{q}_2) = e^{i\mathcal{C}\mathbf{q}_1\times\mathbf{q}_2} t(\mathbf{q}_2)t(\mathbf{q}_1). \quad (36)$$

From the above, we see that translating particles across the whole Brillouin zone commute because $[t(\mathbf{b}_1), t(\mathbf{b}_2)] = 0$. However, they are not the minimal translations that commute with each other. The minimal commuting set is determined by fractional translations by distance $\tilde{\mathbf{b}}_{1,2}$,

$$\tilde{\mathbf{b}}_1 = \mathbf{b}_1/\mathcal{C}_1, \quad \tilde{\mathbf{b}}_2 = \mathbf{b}_2/\mathcal{C}_2. \quad (37)$$

$\tilde{\mathbf{b}}_{1,2}$ thus define a smaller Brillouin zone, which is only a $1/\mathcal{C}$ fraction of the flatband Brillouin zone. Consequently, their real-space unit cell is enlarged by a factor of \mathcal{C} . We denote the real-space lattice vectors as

$$\tilde{\mathbf{a}}_1 = \mathcal{C}_1\mathbf{a}_1, \quad \tilde{\mathbf{a}}_2 = \mathcal{C}_2\mathbf{a}_2. \quad (38)$$

We illustrate an example of the newly introduced lattice vectors with $\mathcal{C} = 2$, $\mathcal{C}_1 = 2$, and $\mathcal{C}_2 = 1$ in Figs. 3(c) and 3(d). As we will see shortly, the new lattice vectors in fact define new degrees of freedom that are crucial in constructing the ideal flatband wave functions and in mapping the flatband to

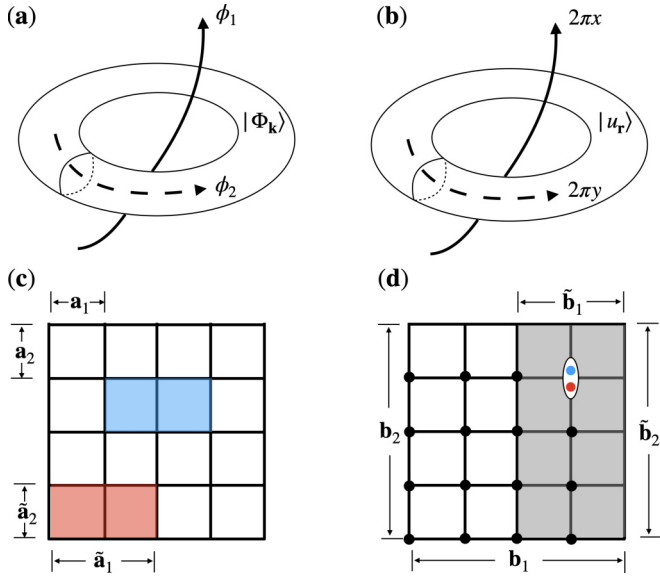


FIG. 3. (a) Inserting boundary condition fluxes $\phi_{1,2}$ pumps the momentum. Such a flux insertion process is generated by the magnetic translation operator in quantum Hall systems. (b) In ideal flatbands, one can define a dual magnetic translation and use the coordinate \mathbf{r} to pump states $|u_{\mathbf{r}}\rangle$. Here $\mathbf{r} = x\mathbf{a}_1 + y\mathbf{a}_2$ with $x, y \in [0, 1)$ is defined within the unit cell spanned by $\mathbf{a}_{1,2}$. (c) Example of the lattice unit cells $\mathbf{a}_{1,2}$ and the enlarged unit cells $\tilde{\mathbf{a}}_{1,2}$ on an $N_1 = N_2 = 4$ system for Chern number $\mathcal{C} = 2$ ($\mathcal{C}_1 = 2, \mathcal{C}_2 = 1$). The blue and red squares are representative magnetic unit cells of the two lowest Landau level states. (d) The momentum-space of the same system, where there are in total $N_1 N_2 = 16$ degrees of freedom representing orthogonal 16 flatband states denoted by the black dots. In mapping to the lowest Landau levels, the first Brillouin zone gets downfolded by \mathcal{C} times into the gray area spanned by $\tilde{\mathbf{b}}_{1,2}$, but each momentum point is enriched by \mathcal{C} colors. The total degrees of freedom are unchanged.

LL physics. Before going into the details of the wave function, we first revisit the boundary condition Eq. (19), which highlights the importance of position-momentum duality and sheds light on the connection between the ideal flatband and LLs.

B. Boundary condition revisited

It is important to notice that the momentum-space boundary condition Eq. (19) in fact can be precisely rewritten in terms of the dual MTG as follows:

$$e^{i\mathbf{b}_i \cdot \hat{\mathbf{Q}}} u_{\mathbf{k}}(\mathbf{r}) = (-1)^{C_i} e^{-i\mathbf{b}_i \cdot \mathbf{r}} u_{\mathbf{k}}(\mathbf{r}). \tag{39}$$

Equation (39) is akin to the boundary condition in quantum Hall problems. Recall that for quantum Hall problems defined on a torus of length $L_{i=1,2}$ consisting of $N_{1,2}$ magnetic unit cells along the two directions, periodic magnetic translation across the torus imposes the following boundary condition for all quantum Hall states $\Phi_{\mathbf{k}}(\mathbf{r})$:

$$e^{iL_i \times \hat{\mathbf{R}} / l_{\tilde{\mathbf{b}}_i}^2} \Phi_{\mathbf{k}}(\mathbf{r}) = (-1)^{N_i} e^{i\phi_i} \Phi_{\mathbf{k}}(\mathbf{r}), \tag{40}$$

where $\phi_{1,2}$ are the boundary condition fictitious fluxes; see, e.g., Fig. 3(a).

It is useful to compare Eq. (39) with Eq. (40). First of all, it is interesting to notice that for ideal flatbands it is the wave function’s coordinate $e^{-i\mathbf{b}_i \cdot \mathbf{r}}$ that tunes the boundary condition of the dual-MTG. Thereby tuning \mathbf{r} generates a Thouless-pump [76] that transports states, analogous to tuning $\phi_{1,2}$ in quantum Hall problems that transport particles. See Figs. 3(a) and 3(b) for a comparison of the “flux insertion process” in Landau levels and ideal flatbands.

In fact, the dual Thouless pump can be numerically verified, for instance by using the chiral twisted multilayer graphene model [38,39]. In Fig. 4, we plotted the absolute value of the ideal flatband wave function $u_{\mathbf{k}}^{\text{Bloch}}(\mathbf{r})$ from the $\mathcal{C} = 2, 3$ model for the top and bottom panel, respectively. We see at any fixed \mathbf{r} that the wave function exhibits \mathcal{C} zeros. Moreover, when we continuously vary \mathbf{r} , the pattern of zeros evolves analogous to charge pumping. There always exists a lattice vector \mathbf{a} such that the indices of zeros get exchanged when $\mathbf{r} \rightarrow \mathbf{r} + \mathbf{a}$. Such a zero exchange phenomenon will immediately become clear when we derive the wave function in the next section.

Lastly, we comment that MTG and dual-MTG differ in many aspects, yet correspondences exist. A comparison between MTG and dual-MTG can be found in Table I. In particular, the Brillouin zone factorization $\mathcal{C}_{1,2}$ in ideal flatbands corresponds to the torus factorization $N_{1,2}$ in Landau levels. This can be understood as follows. In quantum Hall setting, since the LLL wave functions are holomorphic in real-space coordinates and the space has topology of the torus, the wave functions have $N_{\phi} = N_1 N_2$ zeros per the Riemann-Roch theorem. The latter relates the number of zeros to the dimension of the vector space of holomorphic sections of degree N_{ϕ} line bundle. In other words, there are in total N_{ϕ} independent wave functions on the LLL. A similar reasoning applies to ideal flatbands. Due to the Chern number formula, Eq. (12), at any fixed \mathbf{r} the ideal flatband wave function is a holomorphic section of degree \mathcal{C} line bundle, so it will have exactly \mathcal{C} zeros in the first Brillouin zone spanned by $\mathbf{b}_{1,2}$. This implies \mathcal{C} independent solutions satisfying the boundary condition Eq. (19). In the next section, we will construct an explicit basis of the wave functions.

C. Irreducible representation of the dual magnetic translation group

In the end of the last section, we mentioned that there must be \mathcal{C} linearly independent wave functions given the momentum-space boundary condition Eq. (19) as a consequence of the Riemann-Roch theorem. In this section, we use the dual-MTG to derive them. Since wave functions are irreducible representations of the dual-MTG, we start by discussing the representation in general. It is useful to first review the representation in Landau level problems as the dual-MTG shares many similarities with the MTG, although it is also quite different.

1. Landau level and the usual magnetic translation group

We denote the magnetic unit cell by $\tilde{\mathbf{a}}_{1,2}$ too, and we consider a system of length $L_i = N_i \tilde{\mathbf{a}}_i$ for $i = 1, 2$. It will be clear later why we use the same notation as flatbands. Quantum Hall wave functions are labeled by a magnetic momentum \mathbf{k} .

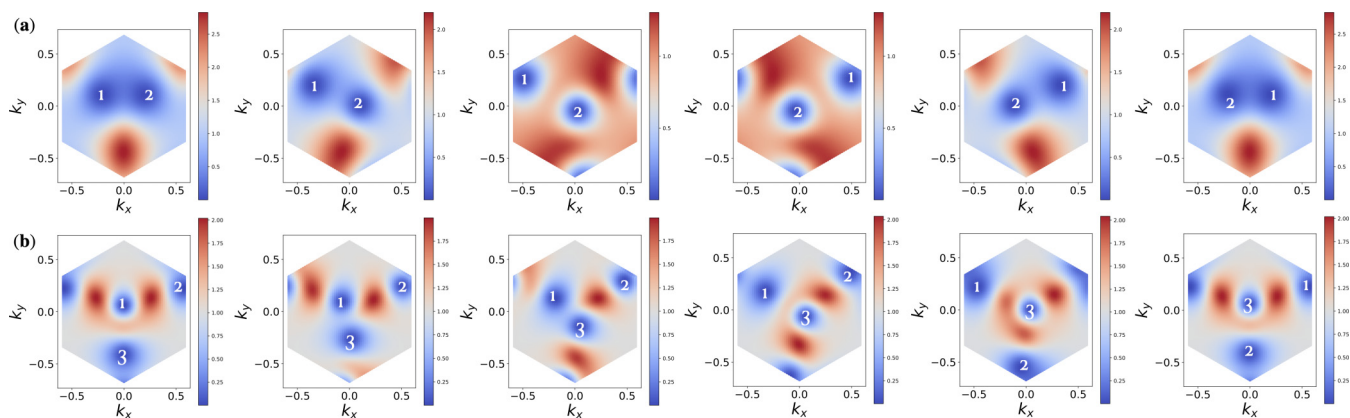


FIG. 4. Momentum-space zeros and their exchanges. Each figure plots $|u_k^{\text{Bloch}}(\mathbf{r})|$ as a function of \mathbf{k} in the Brillouin zone with position \mathbf{r} fixed. For each panel, from left to right, the position \mathbf{r} changes from $\mathbf{r}_0 = (0.5, 0.5)a_M$ to $\mathbf{r}_0 + \mathbf{a}$, where a_M is the moiré lattice constant and \mathbf{a} is a lattice vector. In panel (a), the wave function is taken from the chiral twisted bilayer graphene model ($C = 2$) and $\mathbf{a} = -\mathbf{a}_1 - \mathbf{a}_2$. In panel (b), the wave function is taken from the chiral twisted trilayer graphene model ($C = 3$) and $\mathbf{a} = \mathbf{a}_1$. There are in total C zeros in the Brillouin zone at fixed position \mathbf{r} , and their pattern is lattice translational invariant, but indices can be exchanged. We comment that such nodal structure is only visible when the “unnecessary complications” from the physical layers of the model are removed by the projection procedure defined in Sec. II. The motion of zeros induced by varying position is the dual version of the Thouless pump.

Besides being eigenstates of MTG across the sample Eq. (40), they are also eigenstates by translating $\tilde{\mathbf{a}}_{i=1,2}$:

$$e^{i\tilde{\mathbf{a}}_i \times \mathbf{R} / l_B^2} |\Phi_{\mathbf{k}}\rangle = -e^{i\tilde{\mathbf{a}}_i \cdot \mathbf{k}} |\Phi_{\mathbf{k}}\rangle. \quad (41)$$

We can refer to Eqs. (40) and (41) as the maximal boundary condition and the minimal boundary condition for the quantum Hall problem, respectively. These two boundary conditions together quantize the momentum points onto the lattice shifted by the boundary condition fictitious flux $\phi_{1,2}$:

$$\mathbf{k} = \left(\frac{n_1}{N_1} + \frac{\phi_1}{2\pi} \right) \tilde{\mathbf{b}}_1 + \left(\frac{n_2}{N_2} + \frac{\phi_2}{2\pi} \right) \tilde{\mathbf{b}}_2, \quad (42)$$

where $\tilde{\mathbf{b}}_{1,2}$ are the lattice vectors reciprocal to $\tilde{\mathbf{a}}_{1,2}$.

For a general vector \mathbf{d} allowed by the boundary condition, state $|\Phi_{\mathbf{k}}\rangle$ transforms as

$$e^{i\mathbf{d} \times \mathbf{R} / l_B^2} |\Phi_{\mathbf{k}}\rangle = e^{i\frac{1}{2}\mathbf{d} \cdot \mathbf{k}} |\Phi_{\mathbf{k} + \mathbf{q}_d}\rangle, \quad (43)$$

$$(\mathbf{q}_d)_a \equiv l_B^{-2} \epsilon_{ab} \mathbf{d}^b. \quad (44)$$

It is straightforward to verify that Eq. (43) preserves the magnetic translation algebra.

TABLE I. Comparison of the dual-MTG with the standard one requires a view from position-momentum duality. The flatband Brillouin zone corresponds to the entire real-space torus defining the quantum Hall problem, and fractional flatband Brillouin zone $\tilde{\mathbf{b}}_{1,2}$ corresponds to one magnetic unit cell. There are C dual magnetic unit cells in the flatband problem, and N_ϕ magnetic unit cells in the quantum Hall problem. Interestingly, for ideal flatbands it is the coordinate \mathbf{r} , instead of momentum \mathbf{k} , that tunes the boundary condition and labels representations. The coordinate \mathbf{r} induced charge pump is shown in Fig. 4.

	dual-MTG (for ideal flatbands): $e^{i\mathbf{q} \cdot \mathbf{Q}}$	MTG (for LLs): $e^{i\mathbf{d} \times \mathbf{R} / l_B^2}$
Torus	Brillouin zone; $\mathbf{b}_i = C_i \tilde{\mathbf{b}}_i$; $C = C_1 \times C_2$	Real-space torus; $\mathbf{L}_i = N_i \tilde{\mathbf{a}}_i$; $N_\phi = N_1 \times N_2$
Unit cell	$\tilde{\mathbf{b}}_1 \times \tilde{\mathbf{b}}_2 = 2\pi / (CS)$; $\tilde{\mathbf{a}}_1 \times \tilde{\mathbf{a}}_2 = 2\pi (CS)$	$\tilde{\mathbf{a}}_1 \times \tilde{\mathbf{a}}_2 = 2\pi l_B^2$; $\tilde{\mathbf{b}}_1 \times \tilde{\mathbf{b}}_2 = 2\pi / l_B^2$
Maximal boundary condition	$e^{i\mathbf{b}_i \cdot \mathbf{Q}} u_r\rangle = (-1)^{C_i} e^{i\tilde{\phi}_i} u_r\rangle$	$e^{i\mathbf{L}_i \times \tilde{\mathbf{R}} / l_B^2} \Phi_{\mathbf{k}}\rangle = (-1)^{N_i} e^{i\phi_i} \Phi_{\mathbf{k}}\rangle$
Minimal boundary condition	$e^{i\tilde{\mathbf{b}}_i \cdot \mathbf{Q}} u_r\rangle = -e^{-i\tilde{\phi}_i \cdot \mathbf{r}} u_r\rangle$	$e^{i\tilde{\mathbf{a}}_i \times \mathbf{R} / l_B^2} \Phi_{\mathbf{k}}\rangle = -e^{i\tilde{\mathbf{a}}_i \cdot \mathbf{k}} \Phi_{\mathbf{k}}\rangle$
Representation	$ u_r\rangle$ with $\mathbf{r} = \sum_{i=1,2} (n_i - \tilde{\phi}_i / 2\pi) \tilde{\mathbf{a}}_i / C_i$	$ \Phi_{\mathbf{k}}\rangle$ with $\mathbf{k} = \sum_{i=1,2} (n_i + \phi_i / 2\pi) \tilde{\mathbf{b}}_i / N_i$
Transformation	$e^{i\mathbf{q} \cdot \mathbf{Q}} u_r\rangle = e^{i\frac{1}{2}\mathbf{q} \cdot \mathbf{r}} u_{\mathbf{r} + \mathbf{q}_d}\rangle$	$e^{i\mathbf{d} \times \tilde{\mathbf{R}} / l_B^2} \Phi_{\mathbf{k}}\rangle = e^{i\frac{1}{2}\mathbf{d} \cdot \mathbf{k}} \Phi_{\mathbf{k} + \mathbf{q}_d}\rangle$

The maximal and minimal boundary conditions Eqs. (40) and (41) uniquely determine the expression of the LLL wave function, which is holomorphic in real-space coordinates up to a Gaussian factor [74,75]. The first quantized wave function can be written by the Weierstrass sigma function $\sigma(z)$,

$$\begin{aligned} \Phi_{\mathbf{k}}(\mathbf{r}) &\equiv \langle \mathbf{r} | \Phi_{\mathbf{k}} \rangle \\ &= \sigma(z - z_k) e^{z_k^* z / l_B^2} e^{-\frac{1}{2}|z_k|^2 / l_B^2} e^{-\frac{1}{2}|z|^2 / l_B^2}, \end{aligned} \quad (45)$$

where $z_k = -ikl_B^2$, and $k = \omega^a \mathbf{k}_a$ is the complex momentum coordinate. The Weierstrass sigma function satisfies a quasiperiodic translation property [46,77–79]:

$$\sigma(z + \tilde{\mathbf{a}}_i) = -e^{i\tilde{\mathbf{a}}_i^* (z + \tilde{\mathbf{a}}_i / 2) / l_B^2} \sigma(z), \quad i = 1, 2. \quad (46)$$

2. Basis functions of ideal flatbands and the dual magnetic translation group

Having reviewed the MTG properties for Landau level states, we now proceed to discuss ideal flatband wave functions. We will derive the representation for the dual-MTG in complete analogy to the derivation from Eqs. (41) to (45) used for Landau levels.

The fact that real-space coordinate \mathbf{r} tunes the boundary condition of the dual-MTG motivates us to interpret the ideal flatband wave function as the projection of a quantum state $|u_r\rangle$ into the momentum coordinate space, in complete analogy with quantum Hall wave functions being understood as state $\Phi_{\mathbf{k}}$ labeled by boundary condition \mathbf{k} projected into the real-space as shown in Eq. (45):

$$u_{\mathbf{k}}(\mathbf{r}) = \langle \mathbf{k} | u_r \rangle. \quad (47)$$

Similar to LL wave functions, the ideal flatband states are not only constrained by the maximal boundary condition Eq. (39) but by a minimal boundary condition defined below:

$$e^{i\tilde{b}_i \cdot \mathbf{Q}} |u_r\rangle = -e^{-i\tilde{b}_i \cdot \mathbf{r}} |u_r\rangle. \quad (48)$$

The two boundary conditions, Eqs. (39) and (48), quantize the coordinates \mathbf{r} on a lattice,

$$\mathbf{r} = \left(\frac{m}{\mathcal{C}_1} - \frac{\tilde{\phi}_1}{2\pi} \right) \tilde{\mathbf{a}}_1 + \left(\frac{n}{\mathcal{C}_2} - \frac{\tilde{\phi}_2}{2\pi} \right) \tilde{\mathbf{a}}_2, \quad (49)$$

where $\tilde{\phi}_i$ satisfying $e^{-i\tilde{\phi}_i} = e^{i\tilde{b}_i \cdot \mathbf{r}}$ is precisely the boundary condition for the dual-MTG. For a generic vector \mathbf{q} , the state $|u_r\rangle$ transforms as

$$e^{i\mathbf{q} \cdot \mathbf{Q}} |u_r\rangle = e^{i\frac{1}{2}\mathbf{q} \cdot \mathbf{r}} |u_{\mathbf{r}+\mathbf{r}_q}\rangle, \quad (50)$$

$$(\mathbf{r}_q)^a = \mathcal{C} \epsilon^{ab} q_b. \quad (51)$$

We remind the reader that \mathcal{C} above should be understood as $\mathcal{C}S$ since we have set the unit cell area $2\pi S = 2\pi$ throughout the paper. In this way, $\mathcal{C}S$ has the dimension of area to convert momentum into a coordinate.

The quantization of \mathbf{r} in Eq. (49) implies \mathcal{C} independent states, which are related by lattice translations. Denoting,

$$\mathbf{a}_\sigma \equiv \sigma_1 \mathbf{a}_1 + \sigma_2 \mathbf{a}_2, \quad (52)$$

the first quantized wave functions of the \mathcal{C} independent states can be labeled as

$$v_{\mathbf{k}}^\sigma(\mathbf{r}) \equiv \langle \mathbf{k} | u_{\mathbf{r}+\mathbf{a}_\sigma} \rangle, \quad (53)$$

where $\sigma = (\sigma_1, \sigma_2)$ is the integer-valued color index with $\sigma_i \in [0, \mathcal{C}_i - 1]$.

For notational simplicity, we drop the color index for the $\sigma = (0, 0)$ component. Its wave function is

$$v_{\mathbf{k}}(\mathbf{r}) = \sigma(z - z_k) e^{\frac{1}{2}z_k} e^{-\frac{1}{2\mathcal{C}}|z|^2} e^{-\frac{1}{2\mathcal{C}}|z_k|^2}, \quad (54)$$

where $z_k = -i\mathcal{C}k$. According to Eq. (53), wave functions of other colors are obtained from lattice translations:

$$v_{\mathbf{k}}^\sigma(\mathbf{r}) = v_{\mathbf{k}}(\mathbf{r} + \mathbf{a}_\sigma). \quad (55)$$

It is worth noticing that $e^{i\mathbf{k} \cdot \mathbf{r}} v_{\mathbf{k}}(\mathbf{r})$ is precisely the LLL wave function Eq. (45) of magnetic length $l_B = \sqrt{\mathcal{C}}$. Wave functions with other colors are distinguished by their minimal boundary condition, which we discuss later in the section on mapping a flatband to LLs. We conclude this section with the following comment: all $v_{\mathbf{k}}^\sigma(\mathbf{r})$ obey the required momentum-space boundary condition Eq. (19), which can be straightforwardly verified by using the quasiperiodicity of the sigma function. Thereby, $v_{\mathbf{k}}^\sigma(\mathbf{r})$ are the basis functions spanning the \mathcal{C} -dimensional holomorphic line bundle on the momentum-space manifold for any fixed coordinate \mathbf{r} .

D. General form of ideal flatband wave functions

Although all $v_{\mathbf{k}}^\sigma(\mathbf{r})$ satisfy the required momentum-space boundary condition, they violate the real-space lattice translational invariance, Eq. (18). Thereby, they individually cannot be the wave function for ideal flatbands. In this section, we derive flatband wave functions satisfying both the momentum-space and real-space translational properties.

Since at any fixed \mathbf{r} basis functions $v_{\mathbf{k}}^\sigma(\mathbf{r})$ span the vector space of the holomorphic line bundles specified by the momentum-space boundary condition Eq. (19), the wave function $u_{\mathbf{k}}(\mathbf{r})$ can be definitely written as

$$u_{\mathbf{k}}(\mathbf{r}) = \sum_{\sigma} \mathcal{B}_{\sigma}(\mathbf{r}) v_{\mathbf{k}}^{\sigma}(\mathbf{r}), \quad (56)$$

where $\mathcal{B}_{\sigma}(\mathbf{r})$ is the linear superposition coefficient that varies as a function of \mathbf{r} . For the time being, we assume that $\mathcal{B}_{\sigma}(\mathbf{r})$ of different colors σ are independent functions.

We then impose the real-space boundary condition Eq. (18). The invariance of $u_{\mathbf{k}}(\mathbf{r})$ under lattice translations by $\mathbf{a}_{1,2}$ imposes the following constraints:

$$\mathcal{B}_{\sigma}(\mathbf{r} + \mathbf{a}_1) = \mathcal{B}_{\sigma+(1,0)}(\mathbf{r}), \quad (57)$$

$$\mathcal{B}_{\sigma}(\mathbf{r} + \mathbf{a}_2) = \mathcal{B}_{\sigma+(0,1)}(\mathbf{r}), \quad (58)$$

$$\mathcal{B}_{\sigma}(\mathbf{r} + \tilde{\mathbf{a}}_i) = -e^{-\frac{i}{2\mathcal{C}}\tilde{\mathbf{a}}_i \cdot (\mathbf{r} + \mathbf{a}_\sigma)} \mathcal{B}_{\sigma}(\mathbf{r}). \quad (59)$$

These constrain $\mathcal{B}_{\sigma}(\mathbf{r})$ to have the following form:

$$\mathcal{B}_{\sigma}(\mathbf{r}) \equiv \mathcal{B}(\mathbf{r} + \mathbf{a}_\sigma), \quad (60)$$

$$\mathcal{B}(\mathbf{r} + \tilde{\mathbf{a}}_i) = -e^{-\frac{i}{2\mathcal{C}}\tilde{\mathbf{a}}_i \cdot \mathbf{r}} \mathcal{B}(\mathbf{r}), \quad (61)$$

where $\mathcal{B}(\mathbf{r}) = \mathcal{B}_{\sigma=0}(\mathbf{r})$. Therefore, the wave-function form is uniquely determined by the function $\mathcal{B}(\mathbf{r})$ [80].

Now we have proved that the ideal flatband wave function satisfying the boundary conditions Eqs. (18) and (19) has the general form

$$u_{\mathbf{k}}(\mathbf{r}) = \sum_{\sigma_1=0}^{\mathcal{C}_1-1} \sum_{\sigma_2=0}^{\mathcal{C}_2-1} \mathcal{B}(\mathbf{r} + \mathbf{a}_\sigma) v_{\mathbf{k}}(\mathbf{r} + \mathbf{a}_\sigma), \quad (62)$$

where $\mathcal{B}(\mathbf{r})$ is a \mathbf{k} -independent quasiperiodic function satisfying Eq. (61), and it tunes the Berry curvature. It is now obvious that factorization $\mathcal{C}_{1,2}$ is a gauge choice: a difference choice of factorization affects basis $v_{\mathbf{k}}^\sigma$, whereas $u_{\mathbf{k}}$ is basis-independent. When taking $\mathcal{C} = 1$, the wave function reduces to the form consistent with the result derived in Ref. [24]. Our wave function Eq. (62) is in the explicit first-quantized form and is a generalization of the previously derived ‘‘color-entangled wave function’’ with constant Berry curvature [40–42]. Here ‘‘color’’ refers to the LLL wave functions $v_{\mathbf{k}}^\sigma$, and translations ‘‘entangle’’ them.

Now we comment on the pattern of zeros and their exchanges observed from the wave function of the chiral twisted multilayer graphene model shown in Fig. 4: since lattice translation can permute the color index, zeros are rearranged under one period of such lattice translation; the flatband wave function $u_{\mathbf{k}}$, which is a summation of all color components, remains invariant so the pattern of all zeros is lattice translation periodic.

We can label the location of the \mathcal{C} -zeros in the complex momentum space by $\zeta_{i=1,\dots,\mathcal{C}}(\mathbf{r})$, which are \mathcal{C} smooth functions that map coordinate \mathbf{r} to $k = \omega^a \mathbf{k}_a$. There is an important consistency check we can perform. As a consequence of the Abel theorem, the sum of the positions of the zeros of each of our basis wave functions shall add up to the boundary condition modulo the lattice [81],

$$-i \sum_{i=1}^{\mathcal{C}} \zeta_i(\mathbf{r}) = z \pmod{m_1 a_1 + m_2 a_2}. \quad (63)$$

We anticipate that the zeros $\zeta_i(\mathbf{r})$ will be useful in constructing an explicit first-quantized Halperin-type wave function by regarding index i as layers. We leave this for future exploration.

To conclude this section, relying on the emergent dual guiding centers and their simple algebra, we derived the most general form of a Chern number \mathcal{C} ideal flatband wave function in Eq. (62). It is given by \mathcal{C} LLL-type wave functions entangled by lattice translations. During this derivation, we pointed out the importance of adopting a position-momentum exchanged view for flatbands.

VI. INTERACTING PHYSICS: DENSITY OPERATOR, EXACT GMP ALGEBRA, AND MODEL FRACTIONAL CHERN INSULATORS

Motivated by the unusual numerical observation discussed in Sec. II, in this section we carefully examine the projected density operators and their algebra. Utilizing the universal form of the ideal flatband wave function derived in the previous section, here we explicitly derive the projected density operators and their algebra for all topological ideal flatbands. Importantly, we show that the density operator obeys a closed algebra, generalizing the GMP algebra in a nontrivial way. The generalized GMP algebra is the fundamental reason for the rise of the model FCIs. This result strongly disproved the common lore that fluctuating quantum geometries destabilize FCI-type many-body phases of matter.

A. Definition of the density operator

We define the $\tilde{\mathcal{H}}$ -space projected density operator as follows:

$$\hat{\rho}_q = \sum_k \langle u_{k+q} | u_k \rangle c_{k+q}^\dagger c_k, \quad (64)$$

and we denote the flatband projected density operator as

$$\hat{\rho}_q^{\text{Bloch}} = \sum_k \langle u_{k+q}^{\text{Bloch}} | u_k^{\text{Bloch}} \rangle c_{k+q}^\dagger c_k. \quad (65)$$

Here $u_k \in \tilde{\mathcal{H}}$ and $u_k^{\text{Bloch}} \in \mathcal{H}$ are defined in Eq. (17). These two density operators differ by \mathbf{k} -dependent normalization factors in their matrix element. We will focus on $\hat{\rho}_q$ and will justify why the normalization factor is unimportant for many-body zero modes.

\hat{c}_k^\dagger and \hat{c}_k are the standard particle creation and annihilation operators obeying the standard commutation relation: for fermions we have $\{\hat{c}_k, \hat{c}_{k'}\} = 0$ and for bosons $[\hat{c}_k, \hat{c}_{k'}] = 0$. Since they create/annihilate the wave function u_k , they must

obey a boundary condition inherited from Eq. (19):

$$c_{k+b}^\dagger = \eta_b e^{\frac{i\mathcal{C}}{2} b \times k} c_k^\dagger, \quad (66)$$

where η_b is plus or minus 1: for a vector on the $\tilde{\mathbf{b}}$ -lattice (which of course includes the \mathbf{b} -lattice),

$$\eta_{\tilde{\mathbf{b}}} = (-1)^{m+n+mn} \quad \text{for} \quad \tilde{\mathbf{b}} = m\tilde{\mathbf{b}}_1 + n\tilde{\mathbf{b}}_2. \quad (67)$$

B. Emergent exact GMP algebra at $\mathcal{C} = 1$

We begin with $\mathcal{C} = 1$ ideal flatbands as their color space has a simple unit dimension. We then generalize to generic $\mathcal{C} > 1$ ideal flatbands. We can drop the color index in this case. Reducing Eq. (62) to $\mathcal{C} = 1$, we get its wave function previously derived in Ref. [24]:

$$u_k(\mathbf{r}) = \mathcal{B}(\mathbf{r}) \Phi_k(\mathbf{r}), \quad (68)$$

where $\Phi_k(\mathbf{r})$ is the LLL wave function of magnetic length $l_B = 1$. Since for $\mathcal{C} = 1$ there is no difference between the \mathbf{a} -lattice and the $\tilde{\mathbf{a}}$ -lattice, as implied from Eq. (61), $\mathcal{B}(\mathbf{r})$ is a quasiperiodic function satisfying

$$\mathcal{B}(\mathbf{r} + \mathbf{a}_i) = -e^{-\frac{i}{2} \mathbf{a}_i \times \mathbf{r}} \mathcal{B}(\mathbf{r}). \quad (69)$$

We define a lattice periodic function that admits a Fourier transform as follows:

$$\mathcal{A}(\mathbf{r}) \equiv |\mathcal{B}(\mathbf{r})|^2 = \sum_b \omega_b e^{i\mathbf{b} \cdot \mathbf{r}}, \quad (70)$$

where ω_b are the unique tuning parameters in the $\mathcal{C} = 1$ problem. Equation (68) implies that the flatband form factor can be expressed in terms of LLL form factors:

$$\langle u_k | u_{k'} \rangle = \sum_b \omega_b \langle \Phi_k | e^{i\mathbf{b} \cdot \mathbf{r}} | \Phi_{k'} \rangle = \sum_b \omega_b f_{-b}^{kk'}, \quad (71)$$

where the form factor of the LLL wave function is given below,

$$\begin{aligned} f_{-b}^{kk'} &\equiv \int d^2\mathbf{r} e^{i\mathbf{b} \cdot \mathbf{r}} \Phi_k^*(\mathbf{r}) \Phi_{k'}(\mathbf{r}), \\ &= \eta_b e^{-\frac{i}{2}(\mathbf{k}+\mathbf{k}') \times \mathbf{b} l_B^2} e^{\frac{i}{2} \mathbf{k} \times \mathbf{k}' l_B^2} e^{-\frac{i}{4} |\mathbf{k}-\mathbf{k}'+\mathbf{b}|^2 l_B^2}. \end{aligned} \quad (72)$$

With this form factor, we can rewrite $\hat{\rho}_q$ as follows:

$$\hat{\rho}_q = \sum_b \omega_b \hat{\rho}_{q+b}^{\text{GMP}}, \quad (73)$$

where $\hat{\rho}_q^{\text{GMP}} = \sum_k \int_0^1 c_{k+q}^\dagger c_k$ is the LLL density operator obeying the GMP algebra Eq. (1). In deriving Eq. (73), the boundary condition Eq. (66) is used.

Equation (73) is one of the key results of this section: it shows that the flatband density operator $\hat{\rho}_q$ is obtained from downfolding the LLL density operator into the Brillouin zone, and the downfolding coefficients ω_b are the tuning parameters for the Berry curvature. It also provides an explanation to the exact FQH-type FCIs occurring in the $\mathcal{C} = 1$ ideal flatbands, alternative to the approach from constructing many-body wave functions [30]. To see this, we expand the flatband density-density interaction as

follows:

$$H = \sum_b |\omega_b|^2 \cdot \hat{\rho}_{q+b}^{\text{GMP}} \hat{\rho}_{-q-b}^{\text{GMP}} + \sum_{b \neq 0} \omega_b^2 \cdot \hat{\rho}_{q+b}^{\text{GMP}} \hat{\rho}_{-q+b}^{\text{GMP}} + \sum_{b \neq \pm b'} \omega_b \omega_{b'}^* \cdot \hat{\rho}_{q+b}^{\text{GMP}} \hat{\rho}_{-q-b'}^{\text{GMP}}. \quad (74)$$

The two terms in the first line are the modified relative interaction and the center-of-mass (COM) interaction [24], respectively.

The first term scatters particles by relative momentum $q + b$ while preserving their COM; the strength of interaction is modified by the coefficient ω_b , but the power (range) of the interaction remains unchanged. Therefore, this part cannot modify the zero mode.

The second term represents a new type of interaction: the two-particle interaction depends not only on their relative distance $\hat{R}_- \equiv \hat{R}_1 - \hat{R}_2$ but also on their COM $\hat{R}_+ \equiv \hat{R}_1 + \hat{R}_2$. Since the relative guiding centers commutes with the COM, two sets of independent pseudopotential operators can be constructed,

$$\hat{P}_M^+ = 2 \int \frac{d^2 q l_B^2}{(2\pi)^2} L_M(q^2) e^{-\frac{1}{2} q l_B^2} e^{iq \cdot \hat{R}_+}, \quad (75)$$

$$\hat{P}_m^- = 2 \int \frac{d^2 q l_B^2}{(2\pi)^2} L_m(q^2) e^{-\frac{1}{2} q l_B^2} e^{iq \cdot \hat{R}_-}, \quad (76)$$

where $L_n(x)$ is the n th Laguerre polynomial. Integration over q is replaced with a lattice sum for finite systems. The exact GMP algebra ensures that P^\pm individually are exact projectors that project two particles into their COM angular momentum M and relative momentum m channel, respectively. Since the FQH ground states are exactly annihilated by the relative projectors \hat{P}_m^- and insensitive to the COM projector, the inclusion of such COM interaction also cannot modify the existence of zero modes. The last line of Eq. (74) is a mixture of these two contributions, which also does not affect the interacting zero modes. A more detailed discussion on the COM interaction and the generalized FQH model can be found in Ref. [24].

Last but not least, we justify the statement that ignoring the normalization factor cannot affect the dimension of interacting zero modes. For the unnormalized basis, or generally speaking for the nonorthonormal basis, the eigenequation is described by the following:

$$\sum_\beta H_{\alpha\beta} c_\beta = \lambda \sum_\beta O_{\alpha\beta} c_\beta, \quad (77)$$

where α, β denote the entry of the Hamiltonian, O is the basis overlap matrix, and λ is the eigenvalue. As long as O is fully ranked, the $\lambda = 0$ eigenvalue, if it exists, is unaffected by the concrete form of O . Therefore, we arrive at a useful message for our problem: treating a nonorthonormal system as orthonormal does not affect the dimension of zero modes.

C. Emergent exact GMP algebra at general $C \geq 1$ and a family of model Hamiltonians

The physics of higher Chern bands is enriched by their color degrees of freedom. We start with a discussion about the tuning parameter for the Berry curvature, followed by discussing the general $C \neq 1$ density operators and their algebras.

1. Tuning parameter for Berry curvature

To extract useful information for Berry curvature, we define

$$\mathcal{A}_{\sigma\sigma'}(\mathbf{r}) \equiv e^{\frac{ic}{2} q_\sigma \times q_{\sigma'}} \mathcal{B}_\sigma^*(\mathbf{r}) \mathcal{B}_{\sigma'}(\mathbf{r}) e^{-\frac{ic}{2} (q_\sigma - q_{\sigma'}) \cdot \mathbf{r}}, \quad (78)$$

where

$$(\mathbf{q}_\sigma)_a = C \epsilon_{ab} (\mathbf{a}_\sigma)^b = \left(-\frac{\sigma_1}{C_1} \mathbf{b}_2 + \frac{\sigma_2}{C_2} \mathbf{b}_1 \right)_a. \quad (79)$$

Based on the quasiperiodicity Eq. (61), it is easy to show that \mathcal{A} is $\tilde{\mathbf{a}}$ -lattice translational symmetric satisfying $\mathcal{A}_{\sigma\sigma'}(\mathbf{r}) = \mathcal{A}_{\sigma\sigma'}(\mathbf{r} + \tilde{\mathbf{a}})$. Here $\tilde{\mathbf{a}}$ denotes a generic lattice vector $\tilde{\mathbf{a}} = m\tilde{\mathbf{a}}_1 + n\tilde{\mathbf{a}}_2$. As a consequence, $\mathcal{A}_{\sigma\sigma'}$ can be decomposed into Fourier modes on the $\tilde{\mathbf{b}}$ -lattice:

$$\mathcal{A}_{\sigma\sigma'}(\mathbf{r}) = \sum_{\tilde{\mathbf{b}}} \omega_{\tilde{\mathbf{b}}}(\sigma, \sigma') e^{i\tilde{\mathbf{b}} \cdot \mathbf{r}}. \quad (80)$$

Compared with Eq. (70), the Fourier modes here are enriched by the color indices and are defined on a smaller momentum-space lattice scale. We remind the reader that this is because for $C > 1$ the LLL wave function v_k^g has an enlarged magnetic length $l_B^2 = C$. See Fig. 3(c) for an illustration of the correspondence between flatband and LLL lengthscales.

In fact, not all coefficients $\omega_{\tilde{\mathbf{b}}}(\sigma, \sigma')$ are independent because colors can be related by lattice translations. It turns out after straightforward Fourier transformation analysis that the independent tuning parameters of the system are given by $\omega_{\tilde{\mathbf{b}}}(\mathbf{0}, \delta\sigma)$, where $\delta\sigma \equiv \sigma' - \sigma$ is the color difference taking values from $\delta\sigma_i \in [0, C_i - 1]$. All other components can be generated via

$$\omega_{\tilde{\mathbf{b}}}(\sigma, \sigma + \delta\sigma) = \omega_{\tilde{\mathbf{b}}}(\mathbf{0}, \delta\sigma) e^{iC q_\sigma \times \tilde{\mathbf{b}}}. \quad (81)$$

We therefore can focus on the $\omega_{\tilde{\mathbf{b}}}(\mathbf{0}, \delta\sigma)$ components. Soon we will find that it is particularly convenient to define and use the new notation:

$$\omega_{\tilde{\mathbf{b}}}[\mathbf{q}_{\delta\sigma}] \equiv \omega_{\tilde{\mathbf{b}}}(\mathbf{0}, \delta\sigma). \quad (82)$$

The color space is periodic as the functions \mathcal{B}_σ are all quasiperiodic when \mathbf{r} is advanced by a lattice vector $\tilde{\mathbf{a}}$. This puts another useful relation to the Fourier components that allows us to move from fractional lattice $\tilde{\mathbf{b}}$ to integer lattice \mathbf{b} . Such a relation is

$$\omega_{\mathbf{b}+\tilde{\mathbf{b}}}[\mathbf{q}_{\delta\sigma}] = \eta_{\tilde{\mathbf{b}}} e^{-\frac{ic}{2} \tilde{\mathbf{b}}' \times q_{\delta\sigma}} \omega_{\mathbf{b}}[\mathbf{q}_{\delta\sigma} - \tilde{\mathbf{b}}']. \quad (83)$$

We leave detailed derivations of Eqs. (81) and (83) to the Appendix.

An important implication from Eq. (83) is that, for any lattice vectors $\tilde{\mathbf{b}}$, one can always factorize it into an ‘‘integer part’’ \mathbf{b} living on the \mathbf{b} -lattice and a remaining ‘‘fractional part’’ $\tilde{\mathbf{b}}'$ defined within $\mathbf{b}_{1,2}$, such that $\tilde{\mathbf{b}} = \mathbf{b} + \tilde{\mathbf{b}}'$. Then Eq. (83) states that the fractional lattice dependence can be effectively ‘‘absorbed’’ into the color space. To conclude, we find that the $C > 1$ system is enriched by the color degrees of freedom, and useful information about band geometries is contained either in the set of parameters

$$\{\omega_{\tilde{\mathbf{b}}}(\mathbf{0}, \delta\sigma) \mid \tilde{\mathbf{b}} = m\tilde{\mathbf{b}}_1 + n\tilde{\mathbf{b}}_2; \delta\sigma_i \in [0, C_i - 1]\}, \quad (84)$$

or equivalently in the set of parameters

$$\{\omega_{\mathbf{b}}[\mathbf{q}_{\delta\sigma}] \mid \mathbf{b} = m\mathbf{b}_1 + n\mathbf{b}_2; \delta\sigma_i \in [0, C - 1]\}. \quad (85)$$

We will find $\{\omega_{\bar{b}}(\mathbf{0}, \delta\sigma)\}$ convenient for numerical calculation as the color space is smaller, and $\{\omega_b[\mathbf{q}_{\delta\sigma}]\}$ convenient in analytically deriving the density algebra because of the absence of a fractional lattice \bar{b} -dependence.

2. Family of exact parent Hamiltonians

We proceed to discuss interacting physics in $\mathcal{C} > 1$ ideal flatbands. The explicit form of the wave function and the wave-function overlap enables us to derive the explicit form of the flatband projected interacting Hamiltonian. In this section, we focus on the two-body density-density interaction Eq. (4), but the methods here apply to generic M -body interactions. We derive a family of Hamiltonians, whose Berry curvature is tunable, while all of them preserve model FCIs as the exact zero-energy eigenstates for short-ranged interactions. Therefore, these Hamiltonians are exact parent Hamiltonians for model FCIs. In the following section, we derive the density algebra for general $\mathcal{C} > 1$, and we provide a theoretical understanding for the origin of these model FCIs.

The $\tilde{\mathcal{H}}$ -space projected density operator is defined in Eq. (64). For numerical calculations, all degrees of freedom must be restricted to the $N_1 N_2$ orthogonal states defined within the first Brillouin zone of the flatband. Thereby, we need to use the boundary condition Eq. (19) to convert the momentum of c_k^\dagger appearing in Eq. (64) into the first Brillouin zone. The resulting density-density interacting Hamiltonian for numerical diagonalization study is

$$H = \sum_b \sum_{k_1, \dots, k_4} v_{k_1 - k_4 - b} \mathcal{F}_b^{k_1 k_4} \mathcal{F}_{-b + \delta b}^{k_2 k_3} c_{k_1}^\dagger c_{k_2}^\dagger c_{k_3} c_{k_4}, \quad (86)$$

where $\delta b = k_1 + k_2 - k_3 - k_4$. The \sum_k sums momentum k defined in the first Brillouin zone, while \sum_b sums reciprocal-lattice vectors b of the entire two-dimensional momentum space. In the above, \mathcal{F} is defined and expressed as

$$\begin{aligned} \mathcal{F}_b^{kk'} &= \int d^2 r e^{-i b \cdot r} u_k^*(r) u_{k'}(r) \\ &= \sum_{\sigma \sigma'} \sum_{\bar{b}} \omega_{\bar{b}}(\sigma, \sigma') g_{b-\bar{b}}^{kk'}(\sigma, \sigma'), \end{aligned} \quad (87)$$

and the function g is

$$g_{\bar{b}}^{kk'}(\sigma, \sigma') = e^{\frac{i\mathcal{C}}{2}(-q_\sigma \times q_{\sigma'} + q_\sigma \times k - q_{\sigma'} \times k')} f_{\bar{b}}^{k+q_\sigma, k'+q_{\sigma'}}, \quad (88)$$

where f is the LLL form factor given in Eq. (72) with $l_B^2 = \mathcal{C}$, and $\eta_{\bar{b}}$ is defined in Eq. (67). $\omega_{\bar{b}}(\sigma, \sigma')$ are the tuning parameters of the model discussed in the last section. They are equivalently parametrized by $\omega_b[\mathbf{q}_{\delta\sigma}]$.

Our interacting Hamiltonian Eq. (86) is a generalization of the previously studied color-entangled Hamiltonian [41,42] to allow nonuniform Berry curvature. The model of Ref. [41] has constant Berry curvature and corresponds to setting $\omega_b[\mathbf{q}_{\delta\sigma}] = \delta_{b,0} \delta_{\delta\sigma,0}$ in our model.

We have numerically verified that for all parameters $\omega_b[\mathbf{q}_{\delta\sigma}]$, our model Hamiltonian Eq. (86) exhibits exact $v^{-1} = [(m+1)\mathcal{C} + 1]$ -fold zero-energy degeneracy at filling fraction ν for the short-ranged v_m interaction. Particle-cut entanglement spectra analysis shows that these exact FCIs are Halperin-type states. Moreover, we numerically find

that many-body short-ranged interactions support non-Abelian model FCIs, such as analogs of Read-Rezayi series [82] and a non-Abelian spin-singlet state [83], as exact zero-energy eigenstates for arbitrary $\omega_b[\mathbf{q}_{\delta\sigma}]$, suggesting that the momentum-space complex structure is the origin of exact FCIs for generic M -body repulsions, and it should be a new fundamental property of density operators. In the next sections, we analytically derive the density operator and discuss their hidden exact GMP algebra.

3. Density operator and closed algebra

The general form of a Chern \mathcal{C} ideal flatband wave function is a superposition of \mathcal{C} LLL-type wave functions. Using this fact and the Fourier modes $\omega_b[\mathbf{q}_\sigma]$ defined in the previous section, the density operator can be directly computed. After some algebra detailed in the Appendix, we find that the flatband density operator is given as follows:

$$\hat{\rho}_q = \sum_{\delta\sigma} \sum_b \omega_b[\mathbf{q}_{\delta\sigma}] \hat{\rho}_{q+b}^{\text{GMP}}(\delta\sigma), \quad (89)$$

where \sum' sums color from $\delta\sigma_i \in [0, \mathcal{C} - 1]$. It is downfolded from $\hat{\rho}^{\text{GMP}}$ into the flatband Brillouin zone, and the downfolding coefficient $\omega_b[\mathbf{q}_\sigma]$ is precisely the coefficient that controls the Berry curvature distribution in the flatband problem. The $\hat{\rho}^{\text{GMP}}$ is can be expressed as

$$\hat{\rho}_q^{\text{GMP}}(\delta\sigma) = \sum_k g^{k+q, k}(\delta\sigma) c_{k+q}^\dagger c_k, \quad (90)$$

where $g^{kk'}(\delta\sigma) \equiv g_0^{kk'}(\mathbf{0}, \delta\sigma)$ defined in Eq. (88). The physical meaning of the density operator will be clarified in the next section.

Importantly, $\hat{\rho}^{\text{GMP}}$ obeys a closed algebra of Girvin-MacDonald-Platzman type. Denoting $q \equiv \omega^a q_a$ as the complex variable, we have

$$\begin{aligned} &[\hat{\rho}_{q_1}^{\text{GMP}}(\delta\sigma_1), \hat{\rho}_{q_2}^{\text{GMP}}(\delta\sigma_2)] \\ &= [e^{-\frac{i\mathcal{C}}{2} q_{\delta\sigma_1} \times q_{\delta\sigma_2}} e^{i\mathcal{C}(q_1 - q_{\delta\sigma_1})^* (q_2 - q_{\delta\sigma_2})} - \text{H.c.}] \\ &\quad \times \hat{\rho}_{q_1+q_2}^{\text{GMP}}(\delta\sigma_1 + \delta\sigma_2). \end{aligned} \quad (91)$$

Equations (89) and (91) are key results of this work. They are valid for any system size $N_{1,2}$ and Chern number factorization $\mathcal{C}_{1,2} \geq 1$. They follow directly from the ideal quantum geometric condition Eq. (2) without using any further assumptions [84]. They show how Berry curvature fluctuation (controlled by $\omega_b[\mathbf{q}_\sigma]$) influences the projected density operator and how the exact GMP algebra emerges in the Hilbert space $\tilde{\mathcal{H}}$ of ideal flatbands.

4. Mapping to multilayer Landau levels

In this section, we discuss the physical interpretation of density operator $\hat{\rho}^{\text{GMP}}$, and how the GMP algebra gives rise to exact FCIs. We first recall that the colors, i.e., the basis functions v_k^σ , are related to each other by lattice translations, and each of them has a magnetic unit cell $\tilde{a}_{1,2}$ that encloses an area \mathcal{C} times larger than the lattice unit cell. Thereby, their magnetic Brillouin zone is \mathcal{C} times smaller than the flatband Brillouin zone. For what follows, we assume commensurate geometry such that N_i is divisible by \mathcal{C}_i . Incommensurate

geometries can be easily turned into commensurate geometries by gluing multiple systems together. Such gluing merely changes the spatial periodicity of the interaction, which we argue will not affect interacting zero modes as they are only sensitive to the short-ranged component of interaction. See Figs. 3(c) and 3(d) for an illustration of $C = 2$.

The colors are LLLs of C distinct boundary conditions. To see this, we use them to define Φ_k^σ :

$$\Phi_k^\sigma(\mathbf{r}) \equiv e^{i\mathbf{k}\cdot\mathbf{r}} e^{-\frac{i}{2C}\mathbf{a}_\sigma \times \mathbf{r}} v_k(\mathbf{r} + \mathbf{a}_\sigma), \quad (92)$$

which can be equivalently expressed by

$$\Phi_k^\sigma(\mathbf{r}) = e^{-\frac{iC}{2}\mathbf{q}_\sigma \times \mathbf{k}} \Phi_{\mathbf{k}+\mathbf{q}_\sigma}(\mathbf{r}). \quad (93)$$

They satisfy the following minimal and maximal boundary conditions:

$$e^{i\tilde{\mathbf{b}}_i \cdot \mathbf{R}} |\Phi_k^\sigma\rangle = -e^{-2\pi i \sigma_i / C_i} e^{i\tilde{\mathbf{b}}_i \times \mathbf{k}} |\Phi_k^\sigma\rangle, \quad (94)$$

$$e^{i\mathbf{b}_i \cdot \mathbf{R}} |\Phi_k^\sigma\rangle = (-1)^{C_i} |\Phi_k^\sigma\rangle. \quad (95)$$

This means that given the maximal boundary condition Eq. (95), colors are distinguished by their C different minimal boundary conditions thus living in C different Hilbert spaces \mathcal{H}_σ with $\sigma_i \in [0, C_i - 1]$. Such C spaces \mathcal{H}_σ are not necessarily orthogonal but are independent, thereby fully spanning the flatband Hilbert space \mathcal{H} , and this is an equivalent description of flatband physics. Therefore, when $C > 1$, we are dealing with a problem with multiple boundary conditions. Now we come to a subtlety. Remember that the notion of momentum is itself a gauge choice, i.e., it is dependent on the boundary condition. This is clearly seen from Eq. (93): although v_k^σ or Φ_k^σ is indexed by a momentum \mathbf{k} , their momentum measured from the $\mathcal{H}_{\sigma=\mathbf{0}}$ space is in fact $\mathbf{k} + \mathbf{q}_\sigma$. To clarify, we refer to the momentum measured from the $\sigma = \mathbf{0}$ frame as the ‘‘absolute momentum,’’ and the momentum measured from individual \mathcal{H}_σ as the ‘‘relative momentum.’’ So Φ_k^σ has relative momentum \mathbf{k} and absolute momentum $\mathbf{k} + \mathbf{q}_\sigma$.

The density operator $\hat{\rho}_q^{\text{GMP}}(\delta\sigma)$ then has a simple interpretation: it boosts the absolute momentum of a particle in $\mathcal{H}_{-\sigma'}$ by \mathbf{q} and at the same time maps it into $\mathcal{H}_{-\sigma=-\sigma'+\delta\sigma}$. To see this explicitly, we can rewrite the density operator as

$$\begin{aligned} \hat{\rho}_q^{\text{GMP}}(\sigma' - \sigma) &= \sum_{\mathbf{k}} g^{k+q, k}(\sigma' - \sigma) |\mathbf{k} + \mathbf{q}\rangle \langle \mathbf{k}| \\ &= e^{-\frac{iC}{2}\mathbf{q}_\sigma \times \mathbf{q}_{\sigma'}} \sum_{\mathbf{k}} f^{k+q+q_\sigma, k+q_{\sigma'}} \cdot |\Phi_{\mathbf{k}+q+q_\sigma}^{-\sigma}\rangle \langle \Phi_{\mathbf{k}+q_{\sigma'}}^{-\sigma'}|, \end{aligned} \quad (96)$$

where $|\mathbf{k}\rangle \in \mathcal{H}$ is a flatband state and $|\Phi_{\mathbf{k}}^{-\sigma}\rangle \in \mathcal{H}_{-\sigma}$ is a LLL states, and f is the LLL form factor. We thus justified the meaning of the density operator discussed above.

The resulting interacting Hamiltonian in the LL basis is not standard, however, but interacting zero modes can still be understood. First, the downfolding induced by Berry curvature Eq. (89) implies that there is a center-of-mass interaction in this generalized FQH problem. Such a center-of-mass interaction cannot affect the zero mode for the same reason as explained in the $C = 1$ case discussed in Sec. VIB and

Ref. [24]. Second, different from the layers in LL problems, here colors are not orthogonal. The nonorthogonality also cannot affect zero modes; see the discussions around Eq. (77). Lastly, the density operators in multilayer LL problems are diagonal in layer, whereas in flatbands the density operator is not diagonal in colors. We have numerically verified that this also does not affect the dimension of zero modes.

To conclude this section, using the explicit form of the universal color-entangled wave function provided in Sec. V, in this section we explicitly computed the ideal flatband density operator. We found generally that the flatband density is obtained from downfolding $\hat{\rho}^{\text{GMP}}$ into the flatband Brillouin zone in an exact manner. Importantly, the algebra of $\hat{\rho}^{\text{GMP}}$ is closed, generalizing the previously derived GMP algebra from $C = 1$ LL to the much more general case for ideal flatbands of arbitrary $C > 0$ in a nontrivial way. We demonstrate that the generalized GMP algebra enables an exact mapping from the flatband problem to the multilayered LL problem, where color plays the role of a layer in such mapping. While the resulting multilayered LL problem is still nonstandard in many aspects (exhibiting center-of-mass dependent interactions, nonorthogonal layer degrees of freedom, and a nondiagonal density matrix), we show that neither of them can modify the dimension of many-body zero modes. This summary also answers the two questions posed at the end of Sec. II, which motivated the theory presented in this work.

VII. DISCUSSIONS

Flatband systems are ideal venues to explore strongly interacting phenomena. However, the physics is often complicated by the interactions and by the wave function’s intrinsic geometry, such as Berry curvature. Through systematically studying flatbands in the ideal limit, we derive a general form of a high Chern number Bloch wave function that will be useful for describing various types of quantum phases of matter: on the one hand, our wave function is inherited from the LLL wave function, thus it can naturally express FQH-type fractionalized states; on the other hand, the internal color degree of freedom allows them equally well to describe symmetry-breaking phases. Moreover, we derive a family of exact interacting parent Hamiltonians and point out the hidden closed density algebra. This will provide a general framework and pave the way to thoroughly explore the interplay between the wave function’s geometry and interaction. Our theory also has practical implications for realistic moiré materials and beyond.

First, our results are useful in guiding the experimental search of FCIs in moiré materials. Recently, FCIs were reported in twisted bilayer graphene with weak external fields [34]. The role of ideal quantum geometry in this experiment has been highlighted, mainly motivated by the exact results for the $C = 1$ ideal flatbands in the twisted bilayer graphene at the chiral limit [24,29,30] and numerical results in the realistic parameter regime [35]. The importance of the ideal geometry for general $C > 1$, however, has not been rigorously justified. Our exact results presented in this work set ideal quantum geometry as one of the most crucial indicators [35] for experimental realization of generic FCIs in moiré materials [85–93]. The key message from our results is as follows: optimizing the

single-particle bandwidth and band geometry to approach the ideal condition Eq. (2) should be given high priority before employing heavy numerical computation involving interactions.

Second, recently the momentum-space geometry was found to be important not only for FCIs but also for other phases such as symmetry-breaking states [43], superconductivity [94–97], and others [98–103]. For example, in twisted monolayer/bilayer graphene systems, various topological and nontopological symmetry-breaking states are observed experimentally [34,43]. In particular, half-filling a $\mathcal{C} = 2$ band is experimentally found to have spontaneous translational symmetry breaking to give rise to a topological charge density wave. In a recent exact diagonalization study with realistic interactions, a nearly degenerate continuous manifold of topological charge density waves was reported [92]. Such a topological charge density wave state can be naturally understood from our theory as spontaneous color polarization: as the ideal flatband wave function is a nonlinear superposition of \mathcal{C} LLL states shifted by lattice translations and thus distinguished by their boundary conditions, the real-space charge density wave pattern is a consequence of the polarization in the color space. In general, our single-particle wave function can be regarded as the parent wave function for various daughter states: a generic flatband wave function can be argued to be perturbed from this wave function by breaking the Kähler condition, adding finite dispersion, breaking internal color space symmetries, or others. Apart from quantum Hall related physics, exploring the implication from ideal quantum geometry for flatband superconductivity [94–97,104,105] in double-layer time-reversal symmetric high Chern bands is an interesting future topic.

Besides the wave function, our derived family of interacting Hamiltonians with tunable Berry curvature also deserves future explorations. They are model Hamiltonians with controlled properties: for arbitrary tuning parameters of the Berry curvature, FCIs are exact zero energy as long as the interaction is short-ranged. These model Hamiltonians are thus ideal platforms to explore the intrinsic role of long-ranged parts of the interaction and their interplay with wave-function quantum geometries in determining the ground states and the quantum phase transitions. For instance, in the $\mathcal{C} = 1$ case, a transition from the Laughlin state to a Wigner crystal is proposed to occur in the heterostructure of a Dirac material/type-II superconductor when tuning the range of Coulomb interaction [33]. Richer phase diagrams and phase transitions are expected to occur in high Chern bands and in multilayer moiré materials.

Our theory also opens new directions to the theory of FCI and FQH. Understanding the density operators and their correlations in flatband systems has been a long-term topic [4,22,23,106–110]. As GMP algebra is tightly related to the neutral excitation [14,15,21], it is interesting to ask how Berry curvature fluctuation influences it and the possibility of nematic transitions tuned by geometry, which can be examined based on the theory presented here. Moreover, since in quantum Hall physics the GMP algebra is closely related to other responses such as Hall viscosity [21,66–68,111], we believe the ideal flatband is a natural place to explore this geometric response and beyond in flatband systems [112–114].

Furthermore, our work bridges condensed matter physics and mathematics. Many of our results are motivated and supported by intuitions and rigorous statements from both fields, in particular the quantum Hall and flatband physics, and the Kähler geometry in mathematics. We expect more insights from bridging these two fields in the future. Concretely, the Bergman kernel might be useful to reformulate the density algebra derived in this work, and it offers new perspectives to the emergent pseudopotential projectors. The coherent states in the emergent Hilbert space $\tilde{\mathcal{H}}$ and geometric quantization also deserve further exploration. Moreover, higher-dimensional generalization of ideal flatbands is also an interesting future direction [115–117].

ACKNOWLEDGMENTS

We are grateful to Jennifer Cano, Andrew J. Millis, and Bo Yang for collaboration on $\mathcal{C} = 1$ ideal flatbands [24]. The work of S.K. was partly supported by the IdEx program and the USIAS Fellowship of the University of Strasbourg. Z.L. is supported by the National Key Research and Development Program of China through Grant No. 2020YFA0309200. The Flatiron Institute is a division of the Simons Foundation. This work is also supported by the Center of Mathematical Sciences and Applications at Harvard University.

APPENDIX: SOME USEFUL DERIVATION DETAILS

1. Fourier coefficients

In this section, we discuss the derivation details for Eqs. (81) and (83). Equation (81) follows directly from the following identity:

$$\mathcal{A}_{\sigma,\sigma'}(\mathbf{r}) = \mathcal{A}_{0,\delta\sigma}(\mathbf{r} + \mathbf{a}_\sigma) e^{\frac{i\mathcal{C}}{2} \mathbf{q}_\sigma \times \mathbf{q}_{\sigma'} - \frac{i\mathcal{C}}{2} \mathbf{q}_{\delta\sigma} \cdot \mathbf{a}_\sigma}. \quad (\text{A1})$$

Therefore, the Fourier coefficients $\omega_{\tilde{\mathbf{b}}}(\boldsymbol{\sigma}, \boldsymbol{\sigma}')$ can all be reduced to $\omega_{\tilde{\mathbf{b}}}(\mathbf{0}, \delta\boldsymbol{\sigma})$, which we simply denote as $\omega_{\tilde{\mathbf{b}}}(\delta\boldsymbol{\sigma})$, where $\delta\boldsymbol{\sigma} = \boldsymbol{\sigma}' - \boldsymbol{\sigma}$. Equation (83) follows from

$$\omega_{\tilde{\mathbf{b}}}(\boldsymbol{\sigma} + \mathcal{C}_i \mathbf{e}_i) = -e^{\frac{i}{2\mathcal{C}} \epsilon_{ij} \tilde{\mathbf{b}}_j \times \mathbf{q}_\sigma} \omega_{\tilde{\mathbf{b}} + \epsilon_{ij} \tilde{\mathbf{b}}_j}(\boldsymbol{\sigma}), \quad (\text{A2})$$

which can be obtained by using the quasiperiodicity of $\mathcal{B}(\mathbf{r})$ given in Eq. (61):

$$\mathcal{A}_{0,\sigma + \mathcal{C}_i \mathbf{e}_i}(\mathbf{r}) = -e^{-\frac{i}{2\mathcal{C}} \tilde{\mathbf{a}}_i \times (\mathbf{r} + \mathbf{a}_\sigma)} \mathcal{A}_{0,\sigma}(\mathbf{r}). \quad (\text{A3})$$

2. Form factor

In this section, we show the calculation details of the form factor $\mathcal{F}_b^{kk'}$ defined in the main text. For the $\mathbf{b} = \mathbf{0}$ component, we simply denote it as $\mathcal{F}^{kk'}$. Using the general form of the single-particle wave function, we arrive at

$$\begin{aligned} \mathcal{F}_b^{kk'} &= \sum_{\sigma\sigma'} \int d^2\mathbf{r} e^{-\frac{i\mathcal{C}}{2} \mathbf{q}_\sigma \times \mathbf{q}_{\sigma'}} e^{-i\mathbf{b} \cdot \mathbf{r}} e^{\frac{i}{2} (\mathbf{q}_\sigma - \mathbf{q}_{\sigma'}) \cdot \mathbf{r}} \\ &\quad \times \mathcal{A}_{\sigma\sigma'}(\mathbf{r}) v_k^{\sigma*}(\mathbf{r}) v_k^{\sigma'}(\mathbf{r}), \end{aligned} \quad (\text{A4})$$

where $\mathcal{A}_{\sigma\sigma'}$ is defined in the main text. Then by using

$$v_k^\sigma(\mathbf{r}) = e^{-i(\mathbf{k} + \mathbf{q}_\sigma/2) \cdot \mathbf{r}} e^{-\frac{i\mathcal{C}}{2} \mathbf{q}_\sigma \times \mathbf{k}} \Phi_{\mathbf{k} + \mathbf{q}_\sigma}(\mathbf{r}), \quad (\text{A5})$$

we arrive at the following:

$$\mathcal{F}_b^{kk'} = \sum_{\sigma\sigma'} \sum_{\tilde{b}} \omega_{\tilde{b}}(\sigma, \sigma') e^{\frac{iC}{2}(-q_\sigma \times q_{\sigma'} + q_\sigma \times k - q_{\sigma'} \times k')} \times \langle \Phi_{k+q_\sigma} | e^{i(\tilde{b}-b+k-k'+q_\sigma-q_{\sigma'})\cdot\hat{r}} | \Phi_{k'+q_{\sigma'}} \rangle. \quad (\text{A6})$$

The second line is nothing but the LLL form factor. We summarize the expression for the form factor as follows:

$$\mathcal{F}_b^{kk'} = \sum_{\sigma\sigma'} \sum_{\tilde{b}} \omega_{\tilde{b}}(\sigma, \sigma') g_{b-\tilde{b}}^{kk'}(\sigma, \sigma'), \quad (\text{A7})$$

where functions g and f are

$$g_{\tilde{b}}^{kk'}(\sigma, \sigma') \equiv e^{\frac{iC}{2}(-q_\sigma \times q_{\sigma'} + q_\sigma \times k - q_{\sigma'} \times k')} f_{\tilde{b}}^{k+q_\sigma, k'+q_{\sigma'}}, \quad f_{\tilde{b}}^{kk'} \equiv \eta_{\tilde{b}} e^{\frac{iC}{2}(k+k')\times\tilde{b}} e^{\frac{iC}{2}k\times k'} e^{-\frac{C}{4}|k-k'-\tilde{b}|^2}. \quad (\text{A8})$$

We notice

$$g_{-\tilde{b}}^{kk'}(\sigma, \sigma') = \eta_{\tilde{b}} e^{-\frac{iC}{2}k\times\tilde{b}} e^{-iCq_\sigma\times\tilde{b}} g_{\tilde{b}}^{k+\tilde{b}, k'}(\sigma, \sigma'), \quad (\text{A9})$$

where the index \tilde{b} is omitted for $g_{b=0}^{kk'}$. It is easy to check that $g^{kk'}(\sigma, \sigma')$ depends only on the color difference:

$$g^{kk'}(\delta\sigma) = e^{-\frac{iC}{2}q_{\delta\sigma}\times(k+k')} e^{\frac{iC}{2}k\times k'} e^{-\frac{C}{4}|k-k'-q_{\delta\sigma}|^2}. \quad (\text{A10})$$

3. Density operator

In this section, we derive the expression for the flatband density operator $\hat{\rho}_q \equiv \sum_k \mathcal{F}^{k+q, k} c_{k+q}^\dagger c_k$ and derive their algebra. First, by using Eqs. (81), (A7), (A9), and (A10), the explicit form for the density operator is

$$\hat{\rho}_q = \sum_{\delta\sigma} \sum_{k, \tilde{b}} \eta_{\tilde{b}} e^{-\frac{iC}{2}(k+q)\times\tilde{b}} \omega_{\tilde{b}}(\delta\sigma) g^{k+q+\tilde{b}, k'}(\delta\sigma) \cdot c_{k+q}^\dagger c_k, \quad (\text{A11})$$

where $\sum_{\delta\sigma}$ sums color from $\delta\sigma_i \in [0, C_i - 1]$. Now we further simplify the density operator from the \tilde{b} -lattice to the b -lattice. By using Eq. (83),

$$\omega_{\tilde{b}}(\delta\sigma) = \eta_{\tilde{b}'} e^{-\frac{iC}{2}\tilde{b}'\times q_{\delta\sigma}} \omega_b[\mathbf{q}_{\delta\sigma} - \tilde{b}'], \quad (\text{A12})$$

where $\tilde{b} = \mathbf{b} + \tilde{b}'$, we arrive at the following steps of derivation:

$$\hat{\rho}_q = \sum_{\delta\sigma} \sum_{k, \mathbf{b}, \tilde{b}'} \eta_{\mathbf{b}+\tilde{b}'} e^{-\frac{iC}{2}(k+q)\times(\mathbf{b}+\tilde{b}')} \times \eta_{\tilde{b}'} e^{-\frac{iC}{2}\tilde{b}'\times q_{\delta\sigma}} \omega_b[\mathbf{q}_{\delta\sigma} - \tilde{b}'] \times g^{k+q+\mathbf{b}+\tilde{b}', k}[\mathbf{q}_{\delta\sigma}] \cdot c_{k+q}^\dagger c_k$$

$$= \sum_{\delta\sigma} \sum_{k, \mathbf{b}, \tilde{b}'} \eta_b e^{-\frac{iC}{2}(k+q)\times\mathbf{b}} \times \omega_b[\mathbf{q}_{\delta\sigma} - \tilde{b}'] \times g^{k+q+\mathbf{b}, k}[\mathbf{q}_{\delta\sigma} - \tilde{b}'] \cdot c_{k+q}^\dagger c_k, \quad (\text{A13})$$

where $g^{k+\tilde{b}, k'}(\mathbf{q}_{\delta\sigma}) = e^{-\frac{iC}{2}\tilde{b}\times(k-q_{\delta\sigma})} g^{k, k'}(\mathbf{q}_{\delta\sigma} - \tilde{b})$ and $\eta_{\tilde{b}}\eta_b = \eta_{\tilde{b}+\mathbf{b}} e^{\frac{iC}{2}\tilde{b}\times\mathbf{b}}$ are used. We defined $g^{kk'}[\mathbf{q}_\sigma] \equiv g^{kk'}(\sigma)$. This simplifies the density operator into the following form:

$$\hat{\rho}_q = \sum_{\delta\sigma} \sum_{k, \mathbf{b}} \eta_b e^{-\frac{iC}{2}(k+q)\times\mathbf{b}} \omega_b[\mathbf{q}_{\delta\sigma}] g^{k+q+\mathbf{b}, k}(\delta\sigma) c_{k+q}^\dagger c_k, \quad (\text{A14})$$

where $\sum_{\delta\sigma}$ sums color over $\delta\sigma_i \in [0, C - 1]$. Then using the boundary condition from Eq. (19), $c_{k+q}^\dagger = \eta_b e^{-\frac{iC}{2}\mathbf{b}\times(k+q)} \cdot c_{k+q+b}^\dagger$, we arrive at the final result:

$$\hat{\rho}_q = \sum_{\delta\sigma} \sum_{k, \mathbf{b}} \tilde{\omega}_b[\mathbf{q}_{\delta\sigma}] g^{k+q+\mathbf{b}, k}(\delta\sigma) \cdot c_{k+q+b}^\dagger c_k. \quad (\text{A15})$$

This can be rewritten as

$$\hat{\rho}_q = \sum_{\delta\sigma} \sum_{\mathbf{b}} \tilde{\omega}_b[\mathbf{q}_{\delta\sigma}] \cdot \hat{\rho}_{q+\mathbf{b}}^{\text{GMP}}(\delta\sigma), \quad (\text{A16})$$

where

$$\hat{\rho}_q^{\text{GMP}}(\delta\sigma) \equiv \sum_k g^{k+q, k}(\delta\sigma) \cdot c_{k+q}^\dagger c_k. \quad (\text{A17})$$

We now prove that $\hat{\rho}_q^{\text{GMP}}(\delta\sigma)$ satisfies a closed algebra. To start, we note that independent of particle statistics, the commutator of the density operator is

$$[\hat{\rho}_{q_1}^{\text{GMP}}(\delta\sigma_1), \hat{\rho}_{q_2}^{\text{GMP}}(\delta\sigma_2)] = \sum_k c_{k+q_1+q_2}^\dagger c_k \times [g^{k+q_1+q_2, k+q_2}(\delta\sigma_1) g^{k+q_2, k}(\delta\sigma_2) - (1 \leftrightarrow 2)]. \quad (\text{A18})$$

It is easy to verify that g satisfies a ‘‘chain rule’’:

$$\frac{g^{k+q_1+q_2, k+q_2}(\delta\sigma_1) \cdot g^{k+q_2, k}(\delta\sigma_2)}{g^{k+q_1+q_2, k}(\delta\sigma_1 + \delta\sigma_2)} = e^{-\frac{iC}{2}q_{\delta\sigma_1}\times q_{\delta\sigma_2}} e^{C(q_1-q_{\delta\sigma_1})\cdot(q_2-q_{\delta\sigma_2})}. \quad (\text{A19})$$

We see that the right-hand side is k -independent: this is non-trivial and leads to the closed density algebra shown in the main text after plugging into Eq. (A18).

[1] K. von Klitzing, The quantized Hall effect, *Rev. Mod. Phys.* **58**, 519 (1986).
 [2] H. L. Stormer, D. C. Tsui, and A. C. Gossard, The fractional quantum Hall effect, *Rev. Mod. Phys.* **71**, S298 (1999).
 [3] N. Regnault and B. A. Bernevig, Fractional Chern Insulator, *Phys. Rev. X* **1**, 021014 (2011).
 [4] S. A. Parameswaran, R. Roy, and S. L. Sondhi, Fractional quantum Hall physics in topological flat bands, *C. R. Phys.* **14**, 816 (2013), topological insulators/Isolants topologiques.

[5] E. J. Bergholtz and Z. Liu, Topological flat band models and fractional chern insulators, *Int. J. Mod. Phys. B* **27**, 1330017 (2013).
 [6] T. Neupert, C. Chamon, T. Iadecola, L. H. Santos, and C. Mudry, Fractional (chern and topological) insulators, *Phys. Scr.* **T164**, 014005 (2015).
 [7] Z. Liu and E. J. Bergholtz, Recent developments in fractional Chern insulators, Reference Module in Materials Science and Materials Engineering (2023), doi: 10.1016/B978-0-323-90800-9.00136-0.

- [8] E. Y. Andrei and A. H. MacDonald, Graphene bilayers with a twist, *Nat. Mater.* **19**, 1265 (2020).
- [9] R. Bistritzer and A. H. MacDonald, Moiré bands in twisted double-layer graphene, *Proc. Natl. Acad. Sci. (USA)* **108**, 12233 (2011).
- [10] Y. Cao, V. Fatemi, S. Fang, K. Watanabe, T. Taniguchi, E. Kaxiras, and P. Jarillo-Herrero, Unconventional superconductivity in magic-angle graphene superlattices, *Nature* **556**, 43 (2018).
- [11] Y. Cao, V. Fatemi, A. Demir, S. Fang, S. L. Tomarken, J. Y. Luo, J. D. Sanchez-Yamagishi, K. Watanabe, T. Taniguchi, E. Kaxiras, R. C. Ashoori, and P. Jarillo-Herrero, Correlated insulator behaviour at half-filling in magic-angle graphene superlattices, *Nature* **556**, 80 (2018).
- [12] A. Cappelli, C. A. Trugenberger, and G. R. Zemba, Infinite symmetry in the quantum Hall effect, *Nucl. Phys. B* **396**, 465 (1993).
- [13] S. Iso, D. Karabali, and B. Sakita, Fermions in the lowest Landau level. bosonization, w_∞ algebra, droplets, chiral bosons, *Phys. Lett. B* **296**, 143 (1992).
- [14] S. M. Girvin, A. H. MacDonald, and P. M. Platzman, Collective-Excitation Gap in the Fractional Quantum Hall Effect, *Phys. Rev. Lett.* **54**, 581 (1985).
- [15] S. M. Girvin, A. H. MacDonald, and P. M. Platzman, Magnetoroton theory of collective excitations in the fractional quantum Hall effect, *Phys. Rev. B* **33**, 2481 (1986).
- [16] G. Moore and N. Read, Nonabelions in the fractional quantum Hall effect, *Nucl. Phys. B* **360**, 362 (1991).
- [17] T. H. Hansson, M. Hermanns, S. H. Simon, and S. F. Viefers, Quantum Hall physics: Hierarchies and conformal field theory techniques, *Rev. Mod. Phys.* **89**, 025005 (2017).
- [18] F. D. M. Haldane, Fractional Quantization of the Hall Effect: A Hierarchy of Incompressible Quantum Fluid States, *Phys. Rev. Lett.* **51**, 605 (1983).
- [19] S. A. Trugman and S. Kivelson, Exact results for the fractional quantum Hall effect with general interactions, *Phys. Rev. B* **31**, 5280 (1985).
- [20] S. M. Girvin and T. Jach, Formalism for the quantum Hall effect: Hilbert space of analytic functions, *Phys. Rev. B* **29**, 5617 (1984).
- [21] F. D. M. Haldane, Geometrical Description of the Fractional Quantum Hall Effect, *Phys. Rev. Lett.* **107**, 116801 (2011).
- [22] T. S. Jackson, G. Möller, and R. Roy, Geometric stability of topological lattice phases, *Nat. Commun.* **6**, 8629 (2015).
- [23] R. Roy, Band geometry of fractional topological insulators, *Phys. Rev. B* **90**, 165139 (2014).
- [24] J. Wang, J. Cano, A. J. Millis, Z. Liu, and B. Yang, Exact Landau Level Description of Geometry and Interaction in a Flatband, *Phys. Rev. Lett.* **127**, 246403 (2021).
- [25] M. Claassen, C. H. Lee, R. Thomale, X.-L. Qi, and T. P. Devereaux, Position-Momentum Duality and Fractional Quantum Hall Effect in Chern Insulators, *Phys. Rev. Lett.* **114**, 236802 (2015).
- [26] T. Ozawa and B. Mera, Relations between topology and the quantum metric for chern insulators, *Phys. Rev. B* **104**, 045103 (2021).
- [27] B. Mera and T. Ozawa, Kähler geometry and chern insulators: Relations between topology and the quantum metric, *Phys. Rev. B* **104**, 045104 (2021).
- [28] B. Mera and T. Ozawa, Engineering geometrically flat chern bands with fubini-study kähler structure, *Phys. Rev. B* **104**, 115160 (2021).
- [29] G. Tarnopolsky, A. J. Kruchkov, and A. Vishwanath, Origin of Magic Angles in Twisted Bilayer Graphene, *Phys. Rev. Lett.* **122**, 106405 (2019).
- [30] P. J. Ledwith, G. Tarnopolsky, E. Khalaf, and A. Vishwanath, Fractional chern insulator states in twisted bilayer graphene: An analytical approach, *Phys. Rev. Res.* **2**, 023237 (2020).
- [31] E. Kapit and E. Mueller, Exact Parent Hamiltonian for the Quantum Hall States in a Lattice, *Phys. Rev. Lett.* **105**, 215303 (2010).
- [32] D. Varjas, A. Abouelkomsan, K. Yang, and E. J. Bergholtz, Topological lattice models with constant Berry curvature, *SciPost Phys.* **12**, 118 (2022).
- [33] J. Dong, J. Wang, and L. Fu, Dirac electron under periodic magnetic field: Platform for fractional Chern insulator and generalized Wigner crystal, *arXiv:2208.10516* [cond-mat.mes-hall].
- [34] Y. Xie, A. T. Pierce, J. M. Park, D. E. Parker, E. Khalaf, P. Ledwith, Y. Cao, S. H. Lee, S. Chen, P. R. Forrester, K. Watanabe, T. Taniguchi, A. Vishwanath, P. Jarillo-Herrero, and A. Yacoby, Fractional chern insulators in magic-angle twisted bilayer graphene, *Nature* **600**, 439 (2021).
- [35] D. Parker, P. Ledwith, E. Khalaf, T. Soejima, J. Hauschild, Y. Xie, A. Pierce, M. P. Zaletel, A. Yacoby, and A. Vishwanath, Field-tuned and zero-field fractional Chern insulators in magic angle graphene, *arXiv:2112.13837* [cond-mat.str-el].
- [36] P. J. Ledwith, A. Vishwanath, and D. E. Parker, Vortexability: A unifying criterion for ideal fractional chern insulators, *arXiv:2209.15023* [cond-mat.str-el].
- [37] To clarify different terminologies: “Kähler band” [26–28] refers to a system satisfying Eq. (2) locally for every k where ω_k^{ab} can be momentum-dependent; “ideal band” [24] requires ω^{ab} to be k -independent; “flat Kähler band” further demands constant Berry curvature; “vortexable band” [36] allows non-linear embedding in real space.
- [38] J. Wang and Z. Liu, Hierarchy of Ideal Flatbands in Chiral Twisted Multilayer Graphene Models, *Phys. Rev. Lett.* **128**, 176403 (2022).
- [39] P. J. Ledwith, A. Vishwanath, and E. Khalaf, Family of Ideal Chern Flatbands with Arbitrary Chern Number in Chiral Twisted Graphene Multilayers, *Phys. Rev. Lett.* **128**, 176404 (2022).
- [40] M. Barkeshli and X.-L. Qi, Topological Nematic States and Non-Abelian Lattice Dislocations, *Phys. Rev. X* **2**, 031013 (2012).
- [41] Y.-L. Wu, N. Regnault, and B. A. Bernevig, Bloch Model Wave Functions and Pseudopotentials for All Fractional Chern Insulators, *Phys. Rev. Lett.* **110**, 106802 (2013).
- [42] Y.-L. Wu, N. Regnault, and B. A. Bernevig, Haldane statistics for fractional chern insulators with an arbitrary chern number, *Phys. Rev. B* **89**, 155113 (2014).
- [43] H. Polshyn, Y. Zhang, M. A. Kumar, T. Soejima, P. Ledwith, K. Watanabe, T. Taniguchi, A. Vishwanath, M. P. Zaletel, and A. F. Young, Topological charge density waves at half-integer filling of a moiré superlattice, *arXiv:2104.01178* [cond-mat.str-el].
- [44] J. Behrmann, Z. Liu, and E. J. Bergholtz, Model Fractional Chern Insulators, *Phys. Rev. Lett.* **116**, 216802 (2016).

- [45] J. Dong and E. J. Mueller, Exact topological flat bands from continuum Landau levels, *Phys. Rev. A* **101**, 013629 (2020).
- [46] J. Wang, Y. Zheng, A. J. Millis, and J. Cano, Chiral approximation to twisted bilayer graphene: Exact intravalley inversion symmetry, nodal structure, and implications for higher magic angles, *Phys. Rev. Res.* **3**, 023155 (2021).
- [47] Y. Ren, Q. Gao, A. H. MacDonald, and Q. Niu, WKB Estimate of Bilayer Graphene’s Magic Twist Angles, *Phys. Rev. Lett.* **126**, 016404 (2021).
- [48] G. G. Naumis, L. A. Navarro-Labastida, E. Aguilar-Méndez, and A. Espinosa-Champo, Reduction of the twisted bilayer graphene chiral Hamiltonian into a 2×2 matrix operator and physical origin of flat bands at magic angles, *Phys. Rev. B* **103**, 245418 (2021).
- [49] L. A. Navarro-Labastida and G. G. Naumis, $3/2$ magic angle quantization rule of flat bands in twisted bilayer graphene and its relationship to the quantum Hall effect, *Phys. Rev. B* **107**, 155428 (2023).
- [50] F. K. Popov and A. Milekhin, Hidden wave function of twisted bilayer graphene: The flat band as a Landau level, *Phys. Rev. B* **103**, 155150 (2021).
- [51] O. Vafek and J. Kang, Renormalization Group Study of Hidden Symmetry in Twisted Bilayer Graphene with Coulomb Interactions, *Phys. Rev. Lett.* **125**, 257602 (2020).
- [52] F. Zhang, J. Jung, G. A. Fiete, Q. Niu, and A. H. MacDonald, Spontaneous Quantum Hall States in Chirally Stacked Few-Layer Graphene Systems, *Phys. Rev. Lett.* **106**, 156801 (2011).
- [53] F. R. Geisenhof, F. Winterer, A. M. Seiler, J. Lenz, T. Xu, F. Zhang, and R. T. Weitz, Quantum anomalous Hall effect driven by orbital magnetism in bilayer graphene, *Nature* **598**, 53 (2021).
- [54] Y.-H. Zhang, D. Mao, Y. Cao, P. Jarillo-Herrero, and T. Senthil, Nearly flat Chern bands in moiré superlattices, *Phys. Rev. B* **99**, 075127 (2019).
- [55] Interaction $v_m(\mathbf{q})$ can be equivalently expanded in the Laguerre-Gaussian basis under which the coefficients are also called Haldane pseudopotentials [18]. In the quantum Hall problems, the Laguerre-Gaussian basis is preferred as it is the eigenbasis of two-particle coherent states [18]. We comment that in flatband problems with nonuniform Berry curvature, the association of two-particle coherent states and the Laguerre-Gaussian basis no longer exists, thereby there is no preference between the series expansion shown in Eq. (5) and the Haldane pseudopotential expansion as these two expansion bases are unitary-related.
- [56] This counting can be derived by first considering a \mathcal{C} -layer FQH system and then mapping it to FCI. Suppose this \mathcal{C} -layer FQH system is pierced by N_ϕ magnetic flux, such that there are N_ϕ sectors of the center-of-mass momentum. For bosons with the $v_{m=2n}$ interaction, they feel $n + 1$ Haldane pseudopotentials of even order, which affect both the intralayer and interlayer interactions, and n Haldane pseudopotentials of odd order, which only affect the interlayer interaction. Because there are \mathcal{C} layers, each intralayer pseudopotential has \mathcal{C} copies and each interlayer pseudopotential has $\mathcal{C}(\mathcal{C} - 1)/2$ copies. We know each copy contributes two nonzero energy levels in each of the N_ϕ FQH momentum sectors in the two-particle spectrum, so the total number of nonzero levels is $2(n + 1)[\mathcal{C} + \mathcal{C}(\mathcal{C} - 1)/2] + 2n\mathcal{C}(\mathcal{C} - 1)/2 = \mathcal{C}[(2n + 1)\mathcal{C} + 1]$. Mapping to FCIs, the number of momentum sectors is \mathcal{C} times larger, because we have $N_1 N_2 = \mathcal{C} N_\phi$. So the number of nonzero levels per FCI momentum sector is $\mathcal{C}[(m + 1)\mathcal{C} + 1] = (m + 1)\mathcal{C} + 1$ for bosons. Similarly, we can get the counting for fermions with the $v_{m=2n+1}$ interaction as $(m + 1)\mathcal{C}$.
- [57] A. M. Läuchli, Z. Liu, E. J. Bergholtz, and R. Moessner, Hierarchy of Fractional Chern Insulators and Competing Compressible States, *Phys. Rev. Lett.* **111**, 126802 (2013).
- [58] A. Sterdyniak, C. Repellin, B. A. Bernevig, and N. Regnault, Series of abelian and non-abelian states in $c > 1$ fractional Chern insulators, *Phys. Rev. B* **87**, 205137 (2013).
- [59] Through this work, we use the word “exact FCIs” and “model FCIs” interchangeably: the former refers to the fact that they are exact zero-energy states for short-ranged interactions, and the latter is based on the observation that they also always have infinite large particle-cut entanglement spectra gap [3,38].
- [60] C. H. Lee, M. Claassen, and R. Thomale, Band structure engineering of ideal fractional Chern insulators, *Phys. Rev. B* **96**, 165150 (2017).
- [61] D. Mumford, *Tata Lectures on Theta I* (Birkhäuser, Boston, 2007).
- [62] M. R. Douglas and S. Klevtsov, Bergman kernel from path integral, *Commun. Math. Phys.* **293**, 205 (2010).
- [63] S. Klevtsov, Geometry and large N limits in Laughlin states, [arXiv:1608.02928](https://arxiv.org/abs/1608.02928) [cond-mat.str-el].
- [64] This is equivalent to changing the definition of the L^2 norm of the wave function so that it varies with \mathbf{k} : $\langle \cdot | \cdot \rangle'_{L^2} = \tilde{N}_k^2 \langle \cdot | \cdot \rangle_{L^2}$. The wave functions $u_k(\mathbf{r})$ normalized with the modified L^2 belong to the Hilbert space that we denote as $\tilde{\mathcal{H}}$.
- [65] We write $e^{(s \times t) \cdot \hat{z}}$ as $e^{s \times t}$ throughout the article for simplicity.
- [66] N. Read, Non-abelian adiabatic statistics and Hall viscosity in quantum Hall states and $p_x + ip_y$ paired superfluids, *Phys. Rev. B* **79**, 045308 (2009).
- [67] N. Read and E. H. Rezayi, Hall viscosity, orbital spin, and geometry: Paired superfluids and quantum Hall systems, *Phys. Rev. B* **84**, 085316 (2011).
- [68] A. Gromov and D. T. Son, Bimetric Theory of Fractional Quantum Hall States, *Phys. Rev. X* **7**, 041032 (2017).
- [69] E. Blount, Formalisms of band theory, *Solid State Phys.* **13**, 305 (1962).
- [70] G. Sundaram and Q. Niu, Wave-packet dynamics in slowly perturbed crystals: Gradient corrections and Berry-phase effects, *Phys. Rev. B* **59**, 14915 (1999).
- [71] D. Xiao, M.-C. Chang, and Q. Niu, Berry phase effects on electronic properties, *Rev. Mod. Phys.* **82**, 1959 (2010).
- [72] F. Harper, S. H. Simon, and R. Roy, Perturbative approach to flat Chern bands in the Hofstadter model, *Phys. Rev. B* **90**, 075104 (2014).
- [73] D. Bauer, T. S. Jackson, and R. Roy, Quantum geometry and stability of the fractional quantum Hall effect in the Hofstadter model, *Phys. Rev. B* **93**, 235133 (2016).
- [74] F. D. M. Haldane and E. H. Rezayi, Periodic Laughlin-Jastrow wave functions for the fractional quantized Hall effect, *Phys. Rev. B* **31**, 2529 (1985).
- [75] F. D. M. Haldane, Many-Particle Translational Symmetries of Two-Dimensional Electrons at Rational Landau-Level Filling, *Phys. Rev. Lett.* **55**, 2095 (1985).
- [76] D. J. Thouless, Quantization of particle transport, *Phys. Rev. B* **27**, 6083 (1983).

- [77] F. D. M. Haldane, A modular-invariant modified weierstrass sigma-function as a building block for lowest-landau-level wavefunctions on the torus, *J. Math. Phys.* **59**, 071901 (2018).
- [78] F. D. M. Haldane, The origin of holomorphic states in landau levels from non-commutative geometry and a new formula for their overlaps on the torus, *J. Math. Phys.* **59**, 081901 (2018).
- [79] J. Wang, S. D. Geraedts, E. H. Rezayi, and F. D. M. Haldane, Lattice monte carlo for quantum Hall states on a torus, *Phys. Rev. B* **99**, 125123 (2019).
- [80] These functions can be constructed as follows: $\mathcal{B}(\mathbf{r}) = g(\mathbf{r})v_{k_0}^*(\mathbf{r})$, where $g(\mathbf{r})$ is \tilde{a} -lattice periodic. The k_0 is a fixed, momentum-independent tuning parameter. This gives a concrete way to construct the wave function and to examine their properties. Indeed, the pattern of zeros and their exchange can be numerically verified from wave functions constructed in this way.
- [81] This can be derived based on the explicit wave-function form and by using the momentum-space boundary condition Eq. (19).
- [82] N. Read and E. Rezayi, Beyond paired quantum Hall states: Parafermions and incompressible states in the first excited landau level, *Phys. Rev. B* **59**, 8084 (1999).
- [83] E. Ardonne and K. Schoutens, New Class of Non-Abelian Spin-Singlet Quantum Hall States, *Phys. Rev. Lett.* **82**, 5096 (1999).
- [84] Generalizing to negative Chern number is straightforward as the single-particle wave function is simply complex-conjugated.
- [85] A. Abouelkomsan, Z. Liu, and E. J. Bergholtz, Particle-Hole Duality, Emergent Fermi Liquids, and Fractional Chern Insulators in Moiré Flatbands, *Phys. Rev. Lett.* **124**, 106803 (2020).
- [86] Z. Liu, A. Abouelkomsan, and E. J. Bergholtz, Gate-Tunable Fractional Chern Insulators in Twisted Double Bilayer Graphene, *Phys. Rev. Lett.* **126**, 026801 (2021).
- [87] C. Repellin, Z. Dong, Y.-H. Zhang, and T. Senthil, Ferromagnetism in Narrow Bands of Moiré Superlattices, *Phys. Rev. Lett.* **124**, 187601 (2020).
- [88] C. Repellin and T. Senthil, Chern bands of twisted bilayer graphene: Fractional chern insulators and spin phase transition, *Phys. Rev. Res.* **2**, 023238 (2020).
- [89] H. Li, U. Kumar, K. Sun, and S.-Z. Lin, Spontaneous fractional chern insulators in transition metal dichalcogenide moiré superlattices, *Phys. Rev. Res.* **3**, L032070 (2021).
- [90] V. Crépel and L. Fu, Anomalous Hall metal and fractional Chern insulator in twisted transition metal dichalcogenides, *Phys. Rev. B* **107**, L201109 (2023).
- [91] P. Wilhelm, T. C. Lang, and A. M. Läuchli, Interplay of fractional chern insulator and charge density wave phases in twisted bilayer graphene, *Phys. Rev. B* **103**, 125406 (2021).
- [92] P. Wilhelm, T. C. Lang, M. S. Scheurer, and A. M. Läuchli, Non-coplanar magnetism, topological density wave order and emergent symmetry at half-integer filling of moiré Chern bands, *SciPost Phys.* **14**, 040 (2023).
- [93] M. Claassen, L. Xian, D. M. Kennes, and A. Rubio, Ultrastrong spin-orbit coupling and topological moiré engineering in twisted rrs2 bilayers, *Nat. Commun.* **13**, 4915 (2022).
- [94] S. Peotta and P. Törmä, Superfluidity in topologically nontrivial flat bands, *Nat. Commun.* **6**, 8944 (2015).
- [95] J. Herzog-Arbeitman, A. Chew, K.-E. Huhtinen, P. Törmä, and B. A. Bernevig, Many-Body Superconductivity in Topological Flat Bands, [arXiv:2209.00007](https://arxiv.org/abs/2209.00007) [cond-mat.str-el].
- [96] K.-E. Huhtinen, J. Herzog-Arbeitman, A. Chew, B. A. Bernevig, and P. Törmä, Revisiting flat band superconductivity: Dependence on minimal quantum metric and band touchings, *Phys. Rev. B* **106**, 014518 (2022).
- [97] J. S. Hofmann, D. Chowdhury, S. A. Kivelson, and E. Berg, Heuristic bounds on superconductivity and how to exceed them, *npj Quantum Mater.* **7**, 83 (2022).
- [98] Y. Sheffer and A. Stern, Chiral magic-angle twisted bilayer graphene in a magnetic field: Landau level correspondence, exact wave functions, and fractional chern insulators, *Phys. Rev. B* **104**, L121405 (2021).
- [99] A. Abouelkomsan, K. Yang, and E. J. Bergholtz, Quantum Metric Induced Phases in Moiré Materials, *Phys. Rev. Res.* **5**, L012015 (2023).
- [100] C. Northe, G. Palumbo, J. Sturm, C. Tutschku, and E. M. Hankiewicz, Interplay of band geometry and topology in ideal chern insulators in the presence of external electromagnetic fields, *Phys. Rev. B* **105**, 155410 (2022).
- [101] B. Mera and J. Mitscherling, Nontrivial quantum geometry of degenerate flat bands, *Phys. Rev. B* **106**, 165133 (2022).
- [102] M. Yu, X. Li, Y. Chu, B. Mera, F. N. Ünal, P. Yang, Y. Liu, N. Goldman, and J. Cai, Experimental demonstration of topological bounds in quantum metrology, [arXiv:2206.00546](https://arxiv.org/abs/2206.00546) [quant-ph].
- [103] J. Dong, P. J. Ledwith, E. Khalaf, J. Y. Lee, and A. Vishwanath, Many-body ground states from decomposition of ideal higher Chern bands: Applications to chirally twisted graphene multilayers, *Phys. Rev. Res.* **5**, 023166 (2023).
- [104] F. Xie, Z. Song, B. Lian, and B. A. Bernevig, Topology-Bounded Superfluid Weight in Twisted Bilayer Graphene, *Phys. Rev. Lett.* **124**, 167002 (2020).
- [105] D. Mao and D. Chowdhury, Diamagnetic response and phase stiffness for interacting isolated narrow bands, [arXiv:2209.06817](https://arxiv.org/abs/2209.06817) [cond-mat.str-el].
- [106] X.-L. Qi, Generic Wave-Function Description of Fractional Quantum Anomalous Hall States and Fractional Topological Insulators, *Phys. Rev. Lett.* **107**, 126803 (2011).
- [107] B. Estienne, N. Regnault, and B. A. Bernevig, d -algebra structure of topological insulators, *Phys. Rev. B* **86**, 241104(R) (2012).
- [108] D. N. Sheng, Z.-C. Gu, K. Sun, and L. Sheng, Fractional quantum Hall effect in the absence of landau levels, *Nat. Commun.* **2**, 389 (2011).
- [109] C. Repellin, T. Neupert, Z. Papić, and N. Regnault, Single-mode approximation for fractional chern insulators and the fractional quantum Hall effect on the torus, *Phys. Rev. B* **90**, 045114 (2014).
- [110] G. Murthy and R. Shankar, Hamiltonian theory of fractionally filled chern bands, *Phys. Rev. B* **86**, 195146 (2012).
- [111] B. Bradlyn, M. Goldstein, and N. Read, Kubo formulas for viscosity: Hall viscosity, ward identities, and the relation with conductivity, *Phys. Rev. B* **86**, 245309 (2012).
- [112] T. I. Tügel and T. L. Hughes, Hall viscosity and momentum transport in lattice and continuum models of the integer quan-

- tum Hall effect in strong magnetic fields, *Phys. Rev. B* **92**, 165127 (2015).
- [113] H. Shapourian, T. L. Hughes, and S. Ryu, Viscoelastic response of topological tight-binding models in two and three dimensions, *Phys. Rev. B* **92**, 165131 (2015).
- [114] P. Rao and B. Bradlyn, Hall Viscosity in Quantum Systems with Discrete Symmetry: Point Group and Lattice Anisotropy, *Phys. Rev. X* **10**, 021005 (2020).
- [115] S.-C. Zhang and J. Hu, A four-dimensional generalization of the quantum Hall effect, *Science* **294**, 823 (2001).
- [116] D. Karabali and V. Nair, Quantum Hall effect in higher dimensions, *Nucl. Phys. B* **641**, 533 (2002).
- [117] J. Wang, S. Klevtsov, and M. R. Douglas, Fractional Quantum Hall States on CP² Space, [arXiv:2109.11522](https://arxiv.org/abs/2109.11522) [cond-mat.mes-hall].